Monthly Notices
of the
ROYAL ASTRONOMICAL SOCIETY

MNRAS **428,** 2118–2140 (2013) doi:10.1093/mnras/sts180

The binary fraction of planetary nebula central stars – I. A high-precision, *I*-band excess search

Orsola De Marco,[1,2,3]⋆ Jean-Claude Passy,[4,3] D. J. Frew,[1,2] Maxwell Moe[5] and G. H. Jacoby[6]

[1]*Department of Physics & Astronomy, Macquarie University, Sydney, NSW 2109, Australia*
[2]*Astronomy, Astrophysics and Astrophotonics Research Centre, Macquarie University, Sydney, NSW 2109, Australia*
[3]*Department of Astrophysics, American Museum of Natural History, New York, NY 10024, USA*
[4]*Department of Physics and Astronomy, University of Victoria, Victoria, Canada*
[5]*Department of Astronomy, Harvard University, Cambridge, MA 02138, USA*
[6]*Giant Magellan Telescope and Carnegie Observatories, Pasadena, CA 91101, USA*

Accepted 2012 October 9. Received 2012 October 3; in original form 2012 August 10

ABSTRACT

We still do not know what causes aspherical planetary nebula (PN) morphologies. A plausible hypothesis is that they are due to the presence of a close stellar or substellar companion. So far, only ∼40 binary central stars of PN have been detected, almost all of them with such short periods that their binarity is revealed by photometric variability. Here we have endeavoured to discover binary central stars at any separation, thus determining the unbiased binary fraction of central stars of PN. This number, when compared to the binary fraction of the presumed parent population, can give a first handle on the origin of PN. By detecting the central stars in the *I* band we have searched for cool companions. We have found that 30 per cent of our sample have an *I*-band excess detected between 1 and a few σ, possibly denoting companions brighter than M3–4V and with separations smaller than ∼1000 au. By accounting for the undetectable companions, we determine a debiased binary fraction of 67–78 per cent for all companions at all separations. We compare this number to a main-sequence binary fraction of (50 ± 4) per cent determined for spectral types F6V–G2V, appropriate if the progenitors of today's PN central star population are indeed the F6V–G2V stars. The error on our estimate cannot be constrained tightly, but we determine it to be between 10 and 30 per cent. We conclude that the central star binary fraction may be larger than expected from the putative parent population. However, this result is based on a sample of 27 bona fide central stars and should be considered preliminary. The success of the *I*-band method rests critically on high-precision photometry and a reasonably large sample. From a similar analysis, using the more sensitive *J* band of a subset of 11 central stars, the binary fraction is 54 per cent for companions brighter than ∼M5–6V and with separations smaller than about 900 au. Debiasing this number in the same way as was done for the *I* band we obtain a binary fraction of 100–107 per cent. The two numbers should be the same and the discrepancy is likely due to small-number statistics. Finally, we note how the previously derived short-period PN binary fraction of 15–20 per cent is far larger than expected based on the main-sequence binary fraction and period distribution.

As a byproduct of our analysis we present an accurately vetted compilation of observed main-sequence star magnitudes, colours and masses, which can serve as a reference for future studies. We also present synthetic colours of hot stars as a function of temperature (20–170 kK) and gravity ($\log g = 6$–8) for Solar and PG1159 compositions.

⋆ E-mail: orsola.demarco@mq.edu.au

Key words: techniques: photometric – binaries: general – stars: evolution – white dwarfs – planetary nebulae: general.

1 INTRODUCTION

A single star may be incapable of generating non-spherical planetary nebulae (PN). Models that can reproduce elliptical and bipolar PN shapes (e.g. García-Segura et al. 1999; García-Segura, López & Franco 2005) have traditionally assumed the constancy of magnetic fields over the high-mass-loss period (known as the superwind phase) that characterizes the end of the asymptotic giant branch (AGB) evolution. However, even a weak magnetic field during the end of the AGB can act to slow down the differential rotation that generates the field in the first place: today we have no viable theory to sustain a magnetic field during the superwind phase in a single AGB star (Soker 2006; Nordhaus, Blackman & Frank 2007). An alternative theory, that a binary companion might be responsible for the shaping action, has become central in the study of PN and formed the core of the *binary hypothesis* which postulates that PN form more readily around binaries, where by binary we mean a star accompanied by another star, a brown dwarf or even a planetary system. For a review, see De Marco (2009).

There are several ways in which binary companions as light as planets can alter the shape of the AGB superwind and the subsequent PN (Mastrodemos & Morris 1999; Edgar et al. 2008; Passy et al. 2012). However, this does not prove that all non-spherical PN (about 80 per cent of the entire sample; Parker et al. 2006) derive from a binary interaction. In order to determine the impact of binarity on PN formation a first, fundamental step is to determine the binary fraction of central stars of PN.

Binary detection methods for central stars of PN have centred on the light variability technique, where a central, unresolved binary undergoes eclipses, suffers ellipsoidal distortion or where the cool companion is irradiated by the luminous hot one. This technique is responsible for the detection of almost all the known central star binaries (Bond 2000; Miszalski et al. 2009). The binary fraction determined in this way is ∼15–20 per cent. This technique is biased against binaries with periods longer than about two weeks, against binaries with the orbital plane near the plane of the sky and against companions with small radii (De Marco, Hillwig & Smith 2008).

To determine the binary fraction for binaries with any orbital separation we need a technique that is free of separation biases, such as the detection of red and infrared (IR) excess from photometry or spectroscopy. So far only Zuckerman, Becklin & McLean (1991) and Frew & Parker (2007) have carried out such studies – but also see Bentley (1989) and Holberg & Magargal (2005). Zuckerman et al. (1991) detected definitive *K*-band excess in 50 per cent of 30 central stars but concluded that only in three cases this could be ascribed to a companion, while in the others the emission may be due to hot dust. Frew & Parker (2007) analysed 32 objects with Two Micron All Sky Survey (2MASS) or Deep Near-Infrared Survey of the Southern Sky near-IR photometry and deduced that >53 per cent of PN have a cool companion (the completeness limit of that survey and the error limits were not quantified).

Key to the success of such survey are (i) extremely accurate photometry with well-quantified uncertainties in at least two blue colours (e.g. *B* and *V*, to determine the reddening) and in at least one red colour (*I* or *J*, to detect the excess flux due to the companion); (ii) a sufficiently large sample ($\gtrsim$150 objects) covering the majority of a volume-limited sample and (iii) the use of a red band that is not contaminated by dust, practically leaving only the *I* or *J* band as feasible. Here we present the first paper in a series that uses *I*-band photometry (and *J* where possible) to detect a red or near-IR excess. The *I* band is not as sensitive as the *J* band, but, if photometric errors can be limited to 1 per cent, this method can be a very practical way to observe a substantial number of objects in a relatively short time.

Ideally, we would like to derive the binary fraction and period distribution in separate samples, such as the non-spherical and the spherical subsets of PN. The need for a larger sample as well as the lack of a clear definition of morphological classes leads us to simplify this test: we simply derive the binary fraction (by which, hereafter, we intend the *stellar* binary fraction) among a volume-limited sample of central stars of PN and compare it with that of the presumed main-sequence progenitor population. The expectation from the current scenario, whereby PN derive from stars in the mass range ∼1–8 $M_{\odot}$, whether they are single or in binaries, is that the PN binary fraction should be slightly smaller than that of intermediate-mass main-sequence stars, if companions down to the brown dwarf limit and at all separations can be sampled. A small difference between the binary population on the main sequence and that during the PN phase is justified by the expectation that very close binary main-sequence stars suffer a strong interaction on the red giant branch (RGB) and do not ascend the AGB; also, it is expected that some binary interactions on the RGB or AGB could result in mergers.

The binary fraction of the progenitor population has recently been measured to be (50±4) per cent (Raghavan et al. 2010). This includes *all* companions down to the planetary regime out to all separations with primary stars in the spectral range F6V to G2V. We therefore expect a PN binary fraction of approximately 10 points lower. Clearly, if we are to explain 80 per cent of all PN (those with non-spherical shapes) with a binary interaction, either the binary fraction of PN is higher than that for the main sequence, and close to 80 per cent, or, if it is not, a fraction of PN should be explained by planetary interactions. While testing for the presence of planets around central stars is not generally within reach yet, we start here with determining the *stellar companion*, PN binary fraction.

In Section 2 we describe our sample. In Section 3 we present our observations and data reduction, while in Section 4 we present our measurements of the photometric magnitudes and their uncertainties. In Section 5 we give the details of the technique to detect *I*- and *J*-band excess flux and the predicted accuracies and biases that derive from it. In Section 6 we report our results, including a discussion of objects that were detected to be variable in the course of our observations. A comparison between our results and the prediction for the single and binary scenarios follows in Section 7. In Section 8 we report details of individual objects. We summarize and conclude in Section 9.

2 THE SAMPLE

The goal of this survey is to determine accurate *B*-, *V*- and *I*-band photometry of the ∼200 central stars closest to the Sun. This sample has been recently compiled using the best available data from the literature supplemented by an improved Hα surface brightness–radius relation which allows one to obtain distances accurate to ∼20 per cent in most cases (Frew 2008). Obtaining the *J*-band magnitude of the central stars is also desirable but much less practical for such a large sample.

Table 1. Observational data discussed in Sections 2 and 8.

Name	Sp. type	PN morph.[1]	D (kpc)	M_V (mag)	$E(B-V)$	$T_{\rm eff}$ (method[2]) (K)	log g[3]	Reference & comment
A7	DAO	R?	0.53	6.8	0.00	99 ± 18 (m)	7.03 ± 0.43	Napiwotzki (1999); wide binary
A16	–	R?	2.50	6.3	0.11	95 ± 8 (*Z* He II)	*5.1 or 7.5*	
A20	O(H)	R?	2.35	4.3	0.09	119 ± 22 (m)	6.13 ± 0.13	Rauch et al. (1999)
A28	O(H)	R?	1.10	6.2	0.00	70 ± 30 (*Z* He II)	*5.1 or 7.5*	
A31	DAO	ISM	0.62	6.5	0.04	95 ± 8 (*Z* He II,m)	6.63 ± 0.3	Napiwotzki (1999)
A57	O(H)[a]	E/B	3.0:	4.0:	0.38[b]	>60 (*Z* H I)	*5.0*	[a]Miszalski et al. (2011) [b]Schlafly & Finkbeiner (2011)
A71	–	ISM	1.22	7.7	(0.8)	145 ± 10 (*Z* He II)	*6.2 or 7.0*	
A72	PG1159[c]	E	1.75	4.8	0.09	>100 (*Z* He II)	*5.3 or 7.4*	[c]see Section 8.5
A79	F0V	T/B	3.30	2.5	0.62	165 ± 25 (Tc)	7.3	F0V central star
A84	–	E	1.50	7.3	0.16	101 ± 10 (*Z* He II, Tc)	*5.4 or 7.4*	
DeHt 5	DAO	–	0.35	7.5	0.16	70 ± 10 (m)	6.65 ± 0.19	Napiwotzki (1999); PN mimic
EGB 1	DA	ISM?	0.65	6.7	0.44[b]	147 ± 25 (m)	7.34 ± 0.31	Napiwotzki (1999); PN mimic?
EGB 6	DAO	ISM	0.60	7.0	0.03[b]	110 ± 10 (m)	7.36	Gianninas et al. (2010)
HaWe 5	DA	–	0.42	8.9	0.20	38 ± 2 (m)	7.58 ± 0.20	Napiwotzki (1999); PN mimic
HDW 3	DAO	ISM	0.80	7.0	0.23	125 ± 28 (m)	6.75 ± 0.32	Napiwotzki (1999)
HDW 4	DA	–	0.21	9.6	0.08	47 ± 2 (m)	7.93 ± 0.16	Napiwotzki (1999); PN mimic
IsWe 1	PG1159	ISM	0.63	7.0	–	100 ± 20 (m)	7.0	Werner (1995)
IsWe 2	DA	E	0.95	7.3	–	148 ± 20 (*Z* H I)	*5.4 or 7.4*	
JnEr 1	PG1159	E/B	1.15	6.8	0.06	130 ± 15 (m)	7.0	Rauch & Werner (1995)
K 1-13	–	E/B	2.45	6.4	0.03	80 ± 30 (*Z* He II)	*5.4 or 7.4*	
K 2-2	hgO(H)	ISM?	0.80	4.7	0.03	69 ± 15 (m)	6.09 ± 0.24	Napiwotzki (1999); PN mimic?
NGC 3587	hgO(H)	E	0.78	6.3	0.00	95 ± 8 (m)	6.94 ± 0.31	Napiwotzki (1999)
NGC 6720	DAO	E/B	0.74	6.3	0.08	125 ± 25 (m)	6.88 ± 0.26	Napiwotzki (1999)
NGC 6853	DAO	E/B	0.41	5.9	0.07	130 ± 10 (m)	6.72 ± 0.23	Napiwotzki (1999)
PuWe 1	DAO	R/B?	0.37	7.4	0.09	99 ± 10 (m)	7.09 ± 0.24	see Section 8.18
Sh 2-78	PG1159	E/B	0.75	7.3	0.48	120 ± 15(m)	7.4	Dreizler (1999)
Sh 2-176	DA	ISM	1.0:	7.9	–	150 ± 25 (*Z* He II)	*6.8*	Gianninas et al. (2010)
Sh 2-188	DAO	ISM	0.83	6.9	0.28	130 ± 30 (m)	6.82 ± 0.6	Napiwotzki (1999)
Ton 320	DAO	ISM	0.55	7.0	0.00	78 ± 15 (m)	7.76	see Section 8.21
WeDe 1	DA	ISM	0.79	7.5	–	141 ± 19 (m)	7.53 ± 0.32	Napiwotzki (1999)

[1] Legend – R: round; E: elliptical; B: bipolar; T: torus; ISM: features dominated by interaction with the interstellar medium.
[2] Legend – m: spectral model; *Z* He II: Zanstra method on helium lines; *Z* H I: Zanstra method on hydrogen lines; Tc: cross-over (Ambartsumyan) temperature.
[3] The values in roman font are from stellar atmosphere models, while those in italics are derived from stellar evolutionary tracks, where we have chosen the higher of the two values for our calculations.

The sample presented here consists of 30 central stars of PN which were selected solely based on their low PN surface brightness (radius of the PN is larger than ∼25 arcsec in most cases) as well as on the faint V magnitudes of their central stars. The first criterion allows us to reduce the measurement error; the second insures that fainter companions can be detected because, although faint V magnitudes can imply intrinsically bright, distant objects, the large PN radius tends to select for closer objects whose faint V brightness indicates that the stars are intrinsically faint.

In Tables 1 and 2 we report the best available literature data, as well as values determined here. We used trigonometric distances if available (e.g. Harris et al. 2007; Benedict et al. 2009), otherwise distances were taken from Frew (2008) and Frew et al. (2012). From the distances and dereddened V magnitudes we derived the absolute magnitude, M_V. The effective temperatures are those derived via atmospheric spectrum fitting by several authors. If a model was not available, we adopted the temperature provided by Zanstra analyses of either the hydrogen or helium lines. To do this we used the new V photometry reported here in combination with new integrated Hα fluxes taken from Frew (2008) and Frew et al. (2012). Since these only provide a lower limit to the temperature for optically thin PN, we have used additional information, where appropriate,

Table 2. Near-IR magnitudes from the 2MASS and the UKIRT Infrared Deep Sky Survey (UKIDSS) and Fulbright & Liebert (1993, FL93).

Name	J (mag)	H (mag)	K (mag)	Data source
A7	16.10 ± 0.08	16.16 ± 0.18	>15.08	2MASS
A31	15.95 ± 0.01	15.80 ± 0.01	15.67 ± 0.01	UKIDSS
A72	16.67 ± 0.13	–	–	2MASS
A79	15.05 ± 0.04	14.64 ± 0.06	14.44 ± 0.08	2MASS
DeHt 5	15.57 ± 0.07	15.96 ± 0.20	15.58 ± 0.22	2MASS
EGB 1	16.64 ± 0.16	>17.47	>15.62	2MASS
EGB 6	16.52 ± 0.10	15.95 ± 0.16	16.10 ± 0.26	2MASS
	16.43 ± 0.20	16.08 ± 0.09	15.63 ± 0.04	FL93
HaWe 5	–	–	17.78 ± 0.18	UKIDSS
HDW 3	–	17.62 ± 0.08	17.49 ± 0.12	UKIDSS
K 2-2	14.94 ± 0.05	14.99 ± 0.06	15.09 ± 0.14	2MASS
NGC 3587	16.71 ± 0.13	–	–	2MASS
NGC 6720	16.40 ± 0.20	–	–	2MASS
NGC 6853	14.75 ± 0.05	14.70	14.61	2MASS
Sh 2-78	–	–	17.89 ± 0.15	UKIDSS
Ton 320	16.59 ± 0.16	>15.96	15.73 ± 0.20	2MASS

to determine the most suitable temperature value. The reddening values reported in Table 1 are derived from data in the literature other than the stellar $B - V$ colour, i.e. from the nebular Balmer decrement or using the interstellar hydrogen column density. In Section 5 we will derive the reddening using a comparison of the observed $B - V$ colour and that predicted for a single star of the appropriate temperature. At that time the nebular- and stellar-derived values will be compared.

Out of the 30 objects studied in the *I* band, 3 were later discovered to be PN mimics, nebulae which we exclude to have been ejected by the central star when it was on the AGB (Frew & Parker 2010). These are HaWe 5 and HDW 4, both of which have a very high surface gravity indicating a long cooling age. Such stars departed from the AGB well over the maximum lifetime of a PN of ∼100 000 yr. Their nebulae must be Strömgren spheres ionized by the hot central stars. In addition, we also consider DeHt 5 a PN mimic due to a range of discrepancies which we describe fully in Section 8.8. Although we suspect that two other objects are also PN mimics (EGB 1 and K 2-2), for the moment we keep them in the central star sample. Our *bona fide* sample comprises 27 objects studied in the *I* band of which 11 have additional *J*-band photometry. A79 has a cool spectral type (Rodríguez, Corradi & Mampaso 2001), indicating that it is a binary, but this was not realized at the time of the observations.

In Column 3 of Table 1 we have listed the morphologies of the PN. Many of them are too old and dispersed for a morphology to be determined accurately, and the PN features are dominated by interaction with the interstellar medium (ISM). Those PN we list as 'R?' are approximately round, but may contain internal structure which, in some cases, is distinctly bipolar. An example is A7, which, although diffuse, contains a hint of bipolarity in the form of brighter structure on either side of the star. None of the PN we mark as 'R?' is like the round PN Abell 39 (Jacoby, Ferland & Korista 2001). A20 is a faint round PN with an evacuated cavity around the central star. Its appearance is that of a pole-on doughnut. A28, on the other hand, has a sharp, broken rim and may be more elliptical than round. We will not mention morphology further. It is not a good form, when trying to determine if binarity causes certain morphologies, to use the morphology as an argument for binarity.

3 OBSERVATIONS AND DATA REDUCTION

The observations were acquired during eight nights between 2007 October 30 and November 6 at the 2.1-m telescope at the Kitt Peak National Observatory. However, the data from nights 2 and 8 were not photometric. The weather conditions during the other nights were mostly photometric. Data taken in non-photometric conditions were used to monitor stars for relative variability (see Section 6.1). A log of the observations is presented in Table 3.

The detector was a 2048 × 2048 pixel Tetronix CCD, which was binned 2 × 2 (to achieve a faster readout and reduce the read noise level). The pixel size was 24 μm, and the field of view was 10.2 × 10.2 arcmin^2 [the plate scale is 0.60 arcsec per (binned) pixel]. The electronic gain of the camera was 3.1 e^-/ADU (analogue-to-digital unit), which minimally samples the system noise of 6 e^-, while providing a maximum signal of about 200 000 e^- before saturating.

The observations were made through the *B*, *V*, *R* and *I* Johnson–Cousins astronomical bandpasses. Ten bias frames per night were obtained as well as ten dome flats per filter. Their medians were used to debias and flat-field the exposures. Standard stars were selected from the list of Landolt (1992), so as to encompass the colours and brightnesses of our targets as well as to sample a range of air masses. They are listed in Table 4 alongside with the nights when they were used. We applied a shutter correction of −0.001 s to the header exposure times, very low for even our shortest exposure times.

4 THE DETERMINATION OF THE PHOTOMETRIC MAGNITUDES

Instrumental magnitudes were measured with the APPHOT package in IRAF[1] (Tody 1986, 1993). The radius of the aperture that samples the flux was estimated to be 8 binned pixels by measuring bright stars through increasingly larger apertures. The background was sampled between 8 and 13 binned pixels from the position of the star. Targets were measured using apertures of 3 binned pixels and then aperture corrected. However, it was noticed that the final result was not very different from that obtained by measuring targets through an 8-binned pixel aperture directly with no aperture correction.

The instrumental magnitudes b, v, r and i were then converted to observed magnitudes B, V, R and I on the standard system, by making the following first-order transformation:

$$\begin{aligned} B &= O_B + b + C_B(B - V) - K_B * Z_B \\ V &= O_V + v + C_V(B - V) - K_V * Z_V \\ R &= O_R + r + C_R(V - R) - K_R * Z_R \\ I &= O_I + i + C_I(R - I) - K_I * Z_I, \end{aligned} \tag{1}$$

where O_B, O_V, O_R, O_I are the instrumental offsets, C_B, C_V, C_R, C_i are the colour terms, K_B, K_V, K_R, K_I are the extinction coefficients and Z is the airmass (where the Z values are all the same and the subscripts are there for clarity). There can be a second-order correction due to the atmosphere, and therefore zenith distance because the atmosphere acts as a broad-band colour filter. This second-order correction was negligible. Although the airmass of our observations varied, it was never higher than 2.1 and generally very close to unity.

Our standard stars were used to calculate the needed coefficients. Each standard star was observed through each filter at several values of the airmass, Z, and its instrumental magnitudes b, v, r and i were determined. Then, for each filter, we solved the system of equations in (1) using a least-squares method, where the unknowns are K, C and O. We finally plot $Y_1 = V - O_V - v - C_V(B - V)$ as a function of Z and $Y_2 = I - O_I - i + K_I{}^*Z$ as a function of $R - I$. In Fig. 1, we show the importance of obtaining observations of several standards at different airmass values. When there are a few stars (less than ∼25 stars), the fits tend to be noticeably poorer. The values obtained for each coefficient as well as the total number of stars in each filter are summarized in Table 5.

4.1 Uncertainties

Several precautions are taken to minimize the uncertainty. First, the targets' signal-to-noise ratio is $\gtrsim$100. Secondly, multiple observations of each target are taken on different nights. This guards against possible mistakes in estimating the photometric conditions. It also allows us to assess variability affecting 15–20 per cent of all central stars of PN and usually denoting binarity in its own right (see Section 6.1). Finally, most of our targets have faint, large PN (>25 arcsec), which reduces the error due to background subtraction.

[1] IRAF is distributed by the National Optical Astronomy Observatories, which are operated by the Association of Universities for Research in Astronomy, Inc., under cooperative agreement with the National Science Foundation.

Table 3. Log of observations taken in photometric conditions.

Name	RA	Dec.	Exp times *B*, *V*, *R*, *I* (s)	UT of the observation	Night	Comment
A7	05 03 07.52	−15 36 22.8	60, 60, 60, –	11:22 30/10/2007	1	No *I* band
			45, 45, 45, 90	08:19 03/11/2007	5	
			40, 40, 40, 80	08:35 05/11/2007	7	
A16	06 43 55.46	+61 47 24.7	120, 120, 120, 240	09:56 02/11/2007	4	
			150, 150, 150, 300	07:50 03/11/2007	5	
			120, 120, 120, 240	10:59 04/11/2007	6	
A20	07 22 57.74	+01 45 32.8	120, 120, 120, 240	10:49 02/11/2007	4	
			120, 120, 120, 120, 240	09:02 03/11/2007	5	
			100, 100, 100, 200	09:12 05/11/2007	7	
A28	08 41 35.57	+58 13 48.4	150, 150, 150, 300	10:15 03/11/2007	5	
			120, 120, 120, 240	11:59 04/11/2007	6	
			120, 120, 120, 240	11:38 05/11/2007	7	
A31	08 54 13.16	+08 53 53.0	45, 45, 45, 90	11:24 03/11/2007	5	
			40, 40, 40, 80*2	10:44 05/11/2007	7	
A57	19 17 05.73	+25 37 33.4	100, 100, 100, 150	03:02 02/11/2007	4	
			120, 120, 120, 240	03:42 05/11/2007	7	
A71	20 32 23.22	+47 20 50.4	150, 150, 150, 300	02:52 03/11/2007	5	
			200, 200, 200, 200	04:22 04/11/2007	6	
			250, 250, 250, 500	02:40 05/11/2007	7	
A72	20 50 02.06	+13 33 29.6	80, 80, 80, 80	03:24 01/11/2007	3	
			60, 60, 60, 120	04:59 02/11/2007	4	
			60, 60, 60, 120	04:33 05/11/2007	7	
A79	22 26 17.27	+54 49 38.2	100, 100, 100, 200	04:14 01/11/2007	3	
			100, 100, 100, 200	05:35 02/11/2007	4	
			200, 200, 200, 350	06:19 04/11/2007	6	
A84	23 47 44.02	+51 23 56.9	80, 80, 80, 100	04:51 01/11/2007	3	
			80, 80, 80, 160	06:02 02/11/2007	4	
			120, 120, 120, 240	05:24 05/11/2007	7	
DeHt 5	22 19 33.73	+70 56 03.1	50, 50, 50, 80	03:52 02/11/2007	4	
EGB 1	01 07 07.59	+73 33 23.2	80, 80, 80, 160	06:54 02/11/2007	4	
			80, 80, 80, 160	03:52 03/11/2007	5	
EGB 6	09 52 58.99	+13 44 34.9	60, 60, 60, 120	12:13 02/11/2007	4	
			60, 60, 60, 120	11:09 05/11/2007	7	
HaWe 5	03 45 26.642	+37 48 51.7	100, 100, 100, 200	08:40 02/11/2007	4	
			100, 100 100. 200	05:34 03/11/2007	5	
HDW 3	03 27 15.44	+45 24 20.5	120,120, 120, 240	07:40 30/10/2007	1	
			160, 160, 160, 320	08:01 02/11/2007	4	
			100, 100, 100, 200	06:47 05/11/2007	7	
HDW 4	05 37 56.23	+55 32 16.0	120, 120, 120, 240	09:30 02/11/2007	4	Clear?
IsWe 1	03 49 05.89	+50 00 14.8	120, 120, 120, 240	05:29 03/11/2007	5	
			100, 100, 100, 200	06:58 04/11/2007	6	
			100, 100, 100, 200	07:12 05/11/2007	7	
IsWe 2	22 13 22.53	+65 53 55.5	80, 80, 80, 160	03:48 01/11/2007	3	
			80, 80, 80, 160	04:13 02/11/2007	4	*I* band done later at 4:53
			80, 80, 80, 160	03:25 03/11/2007	5	
			150, 150, 150, 250	05:47 04/11/2007	6	
			100, 100, 100, 200	04:59 05/11/2007	7	
JnEr 1	07 57 51.63	+53 25 17.0	120, 120, 120, 120	11:20 02/11/2007	4	
			100, 100, 100, 200	09:43 05/11/2007	7	
K 1-13	08 06 46.50	−02 52 34.8	150, 150, 150, 250	11:54 01/11/2007	3	
			120, 120, 120, 200	11:43 02/11/2007	4	
			150, 150, 150, 250	11:50 03/11/2007	5	
K 2-2	06 52 23.17	+09 57 55.7	30, 30, 30, 60	10:29 02/11/2007	4	
			30, 30, 30, 60	08:41 03/11/2007	5	
			30, 30, 30, 60	08:57 05/11/2007	7	
NGC 3587	11 14 47.73	+55 01 08.5	60, 60, 60, 120	12:35 02/11/2007	4	
			60, 60, 60, 120	12:27 04/11/2007	5	
			60, 60, 60, 120	12:41 05/11/2007	6	
NGC 6720	18 53 35.08	+33 01 45.0	50, 50, 50, 50	01:59 02/11/2007	4	
			30, 30, 30, 60	03:23 05/11/2007	7	

Table 3 – *continued*

Name	RA	Dec.	Exp times *B*, *V*, *R*, *I* (s)	UT of the observation	Night	Comment
NGC 6853	19 59 36.38	+22 43 15.7	15, 15, 15, 15	03:32 02/11/2007	4	
			30, 30, 30, 60	02:34 03/11/2007	5	
			20, 20, 20, 40	04:13 05/11/2007	7	
PuWe 1	06 19 34.33	+55 36 42.3	50, 50, 50, 100	07:25 03/11/2007	5	
			50, 50, 50, 100	07:40 05/11/2007	7	
Sh 2-78	19 03 10.09	+14 06 58.9	100, 100, 100, 150	02:32 02/11/2007	4	
			150, 120, 120, 400	01:58 03/11/2007	5	
Sh 2-176	00 31 54	+57 22.6	80, 80, 80, 160	05:17 01/11/2007	3	
			80, 80, 80, 160	06:27 02/11/2007	4	
			150, 150, 150, 300	05:50 05/11/2007	7	
Sh 2-188	01 30 33.11	+58 24 50.7	120, 120, 120, 240	07:16 02/11/2007	4	
			120, 120, 120, 240	04:17 03/11/2007	5	
			120, 120, 120, 240	06:21 05/11/2007	7	
Ton 320	08 27 05.53	+31 30 08.6	60, 60, 60, 120	09:42 03/11/2007	5	
			60, 60, 60, 180	10:15 05/11/2007	7	
WeDe 1	05 59 24.87	+10 41 40.4	120, 120, 120, 240	06:53 03/11/2007	5	
			120, 120, 120, 240	11:31 04/11/2007	6	
			120, 120, 120, 240	08:05 05/11/2007	7	

Table 4. Coefficients and errors for every photometric night. As explained in Section 3, nights 2 and 8 were non-photometric.

Coeff.	Night 1	Night 3	Night 4	Night 5	Night 6	Night 7
O_B	−0.8638 ± 0.0083	−0.8209 ± 0.0157	−0.8436 ± 0.0080	−0.8525 ± 0.0088	−0.9012 ± 0.0153	−0.8466 ± 0.0079
O_V	−0.8054 ± 0.0073	−0.7767 ± 0.0168	−0.7877 ± 0.0100	−0.7958 ± 0.0069	−0.8155 ± 0.0167	−0.7970 ± 0.0064
O_R	−0.7940 ± 0.0068	−0.6169 ± 0.0244	−0.7656 ± 0.0127	−0.7824 ± 0.0140	−0.7775 ± 0.0193	−0.7887 ± 0.0127
O_I	−1.774 ± 0.008	−1.790 ± 0.038	−1.756 ± 0.013	−1.778 ± 0.017	−1.758 ± 0.035	−1.752 ± 0.013
K_B	0.2286 ± 0.0059	0.2550 ± 0.0107	0.2370 ± 0.0054	0.2355 ± 0.0056	0.2205 ± 0.0106	0.2522 ± 0.0055
K_V	0.1313 ± 0.0050	0.1445 ± 0.0113	0.1373 ± 0.0070	0.1325 ± 0.0043	0.1441 ± 0.0101	0.1464 ± 0.0042
K_R	0.090 11 ± 0.004 68	0.2310 ± 0.0165	0.1011 ± 0.0091	0.081 12 ± 0.008 86	0.1072 ± 0.0178	0.093 76 ± 0.008 63
K_I	0.047 85 ± 0.005 37	0.052 81 ± 0.026 54	0.042 64 ± 0.009 56	0.013 15 ± 0.011 01	0.046 23 ± 0.022 83	0.048 95 ± 0.009 35
C_B	0.028 32 ± 0.003 20	0.030 06 ± 0.005 46	0.02772 ± 0.003 08	0.032 48 ± 0.002 98	0.028 49 ± 0.006 00	0.027 47 ± 0.002 73
C_V	−0.030 70 ± 0.002 64	−0.029 54 ± 0.006 07	−0.031 41 ± 0.003 35	−0.034 80 ± 0.002 32	−0.034 65 ± 0.006 70	−0.031 37 ± 0.002 54
C_R	−0.035 81 ± 0.004 72	−0.059 41 ± 0.014 34	−0.044 64 ± 0.007 54	−0.068 85 ± 0.006 96	−0.1066 ± 0.0125	−0.069 55 ± 0.008 04
C_I	0.051 39 ± 0.005 86	−0.2063 ± 0.0161	0.031 63 ± 0.009 44	−0.069 26 ± 0.011 15	−0.1347 ± 0.0258	−0.029 35 ± 0.009 43
No. of stars (*B*, *V*, *R*, *I*)	27, 28, 24, 23	21, 18, 11, 9	54, 47, 35, 27	46, 49, 33, 35	24, 28, 22, 25	50, 63, 54, 50

The uncertainties on the instrumental magnitude measurements (σ_b, σ_v, σ_r and σ_i) provided by IRAF include the photon statistics and the uncertainty on the sky measurement. While the shutter correction was included, we did not include a shutter correction error because it was deemed negligible. By adding the uncertainties in quadrature we have, e.g., in the case of the error on the *B*-band magnitude

$$\sigma_B^2 = \sigma_{O_B}^2 + \sigma_b^2 + (B-V)^2\sigma_{C_B}^2 + C_B^2\sigma_{B-V}^2 + Z_B^2\sigma_{K_B}^2 + \sigma_{\rm apco}^2$$

where $\sigma_{\rm apco} \approx 0.004$ mag is the error on the aperture correction, calculated as the standard deviation of the aperture correction for the five reference stars used to calculate the aperture correction itself. By adopting the approximation $\sigma_{B-V}^2 = \sigma_B^2 + \sigma_V^2 \approx 2\sigma_V^2$, we obtain the following equations for the errors on the *B* and *V* bands:

$$\sigma_B^2 = \left(\sigma_{O_B}^2 + \sigma_b^2 + (B-V)^2\sigma_{C_B}^2 + Z_B^2\sigma_{K_B}^2 + \sigma_{\rm apco}^2\right) \Big/ \left(1 - 2C_B^2\right) \quad (2)$$

$$\sigma_V^2 = \left(\sigma_{O_V}^2 + \sigma_v^2 + (B-V)^2\sigma_{C_V}^2 + Z_V^2\sigma_{K_V}^2 + \sigma_{\rm apco}^2\right) \Big/ \left(1 - 2C_V^2\right),$$

which we solve simultaneously to derive the values of σ_B and σ_V. Similarly, we derive the uncertainties on *R* and *I*.

When more than one independent observation was taken for a given target, the weighted mean was calculated,

$$\mu = \sum_{i=1}^{N} p_i x_i, \quad (3)$$

where *N* is the number of observations, x_i is a given measurement and p_i is its associated probability [$p_i = (1/\sigma_i)/\Sigma_j(1/\sigma_j)$, where σ_i is the error on that measurement and σ_j is the error on the *j*th measurement]. The error on the mean was calculated in the following way:

$$\sigma = \sqrt{\sum_{i=1}^{N} p_i (x_i - \mu)^2}. \quad (4)$$

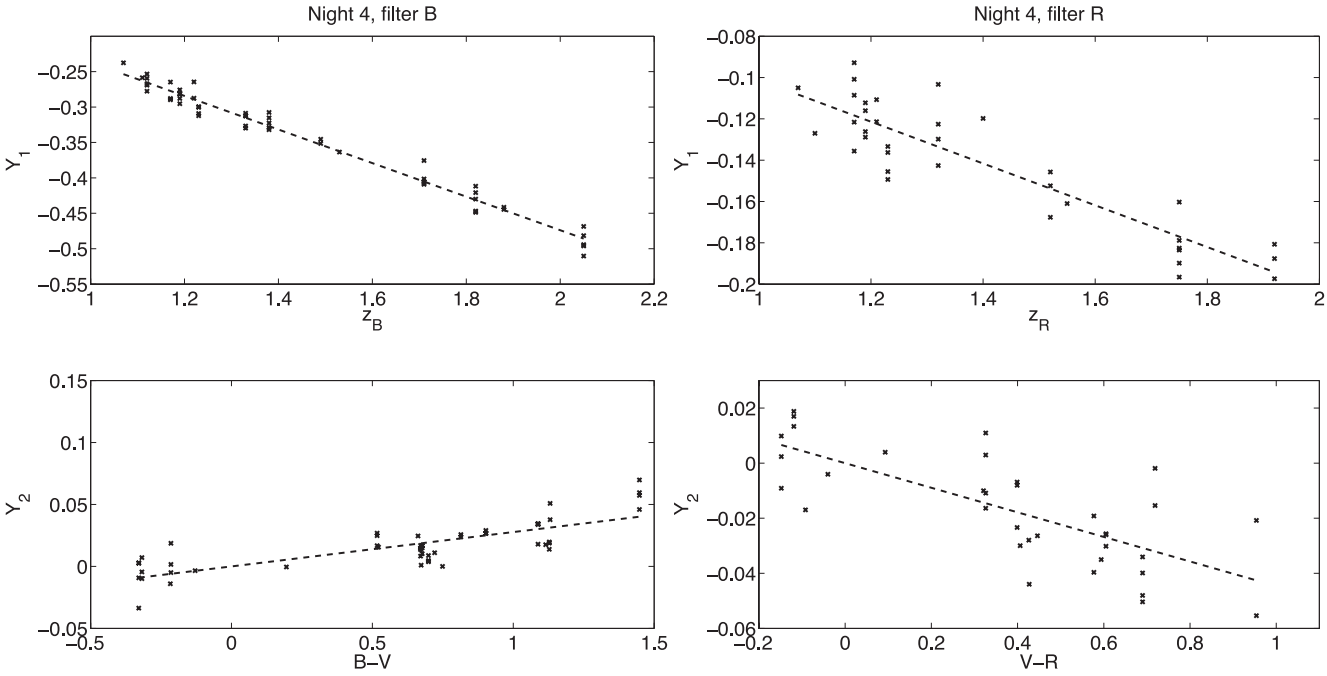

Figure 1. Example of fits to standard stars to estimate conversion coefficients. Note the small range on the *y*-axis of the *R*-band fit.

Table 5. Standard stars from Landolt (1992, 2009). In Column 2 we indicate the number of blue stars (marked 'B'), as well as of redder stars.

Name	No. of stars	Night observed
GD 246	1B	1, 3, 4, 5, 6, 7
PG0231+051	1B + 6	1, 3, 4, 5, 6, 7
PG0918+029	1B + 4	5
PG1047+003	1B + 3	5
PG2213−006	1B + 3	3, 4, 5, 6, 7
RU 149	2B + 6	1, 4, 5, 6, 7
92 245[a]	4	1, 3, 4, 5, 6, 7
95 112[b]	1B + 4	1, 3, 4, 5, 6, 7
98 650[c]	1B + 9	1, 3, 4, 5, 6, 7

[a]This field also contains 92 248, 92 249 and 92 250.
[b]This field also contains 95 41–43 and 95 115.
[c]This field also contains 98 653, 98 670–671, 98 675–676, 98 L5, 98 682, 98 685 and 98 1087.

The photometric magnitudes and their errors thus obtained are reported in Table 6, along with the number of measurements that were used in obtaining these values. In Appendix A (Table A1) we report the individual values and their individual errors.

5 BINARY DETECTION TECHNIQUE BY RED AND IR EXCESS FLUX

The ideal spectral location for this technique is the *J* band. This is the best compromise between companion brightness and the elimination of contamination from hot dust. However, procuring *J*-band data has proven more challenging than optical data because IR instruments are often associated with larger telescopes which tend to allocate shorter observing runs and because of the need for photometric conditions. In addition, for most of our sample we also need to obtain *B*- and *V*-band photometry because the values in the literature do not tend to be sufficiently accurate, thus generating the need for parallel proposals to more than one telescope. As a result, we have found it more practical to use the *I* band to detect companion-generated flux excess as our work horse, accompanied by the *J* band when available [we used the United Kingdom Infrared Telescope (UKIRT) Infrared Deep Sky Survey (UKIDSS; Lawrence et al. 2007) data, or the most reliable 2MASS values – see Table 2]. Below we discuss the technique and its biases.

Most of our targets have reasonably well-determined effective temperatures either via stellar spectrum modelling or using the Zanstra technique (Table 1). Those that were modelled also have known gravities. For those stars with only a Zanstra temperature estimate, we determine the gravity using the most common central star mass, namely 0.61 $M_{\odot}$, selecting the corresponding stellar evolutionary track from fig. 2 of Napiwotzki (1999, who used tracks from Schönberner (1983), Koester & Schönberner (1986) and Blöcker (1995)) and choosing the larger of the possible gravity values, appropriate for our sample of evolved PN. Once the temperatures are obtained, single-star colours ($B - V$, $V - I$ and $V - J$) can be predicted. The predicted $B - V$ colour is used together with the measured one to determine the reddening, $E(B - V)$. If the reddening thus determined has a negative value, possible because of random errors, we set the value to zero. As we will see in Section 6, all negative reddening values we derive in this way are very small and within the uncertainty, reassuring us that the uncertainties have been assessed reasonably. With the reddenings thus derived we obtain values of $A_{\lambda}/E(B - V)$ using the reddening law of Cardelli, Clayton & Mathis (1989), where λ represent the bandpass central wavelengths. The central wavelengths for the filter bandpasses are obtained by convolving the bandpasses with a synthetic stellar atmosphere with $T_{\rm eff} = 100$ kK, $\log g = 7$ and solar abundance. This decreases the central wavelengths by approximately 10 Å, compared to the values obtained for unconvolved bandpasses, but yields only a very small change in the

Table 6. The photometric magnitudes of our targets rounded to three decimal places. Formal errors lower than 1 per cent were set at 1 per cent. In parentheses is the number of independent exposures (taken on different nights) used to calculate the final photometric magnitude and the uncertainty. In Table A1 we present the individual magnitudes whose weighted averages are displayed here.

Name	*B*	*V*	*R*	*I*
A7	15.190 ± 0.003(3)	15.495 ± 0.004(3)	15.632 ± 0.013(3)	15.818 ± 0.011(2)
A16	18.517 ± 0.015(3)	18.714 ± 0.018(3)	18.733 ± 0.020(3)	18.686 ± 0.016(3)
A20	16.216 ± 0.002(3)	16.466 ± 0.006(3)	16.559 ± 0.007(3)	16.701 ± 0.016(3)
A28	16.280 ± 0.008(3)	16.557 ± 0.009(3)	16.691 ± 0.008(3)	16.877 ± 0.014(3)
A31	15.201 ± 0.007(2)	15.544 ± 0.001(2)	15.693 ± 0.009(2)	15.831 ± 0.016(2)
A57	17.903 ± 0.001(2)	17.734 ± 0.011(2)	17.451 ± 0.010(2)	17.210 ± 0.002(2)
A71	19.384 ± 0.015(3)	19.335 ± 0.006(3)	19.253 ± 0.010(3)	19.185 ± 0.056(3)
A72	15.761 ± 0.021(3)	16.070 ± 0.028(3)	16.237 ± 0.091(3)	16.381 ± 0.043(3)
A79	17.825 ± 0.013(3)	16.965 ± 0.005(3)	16.397 ± 0.026(3)	15.743 ± 0.085(3)
A84	18.366 ± 0.012(3)	18.584 ± 0.013(3)	18.613 ± 0.020(3)	18.671 ± 0.020(3)
DeHt 5	15.268 ± 0.018(1)	15.495 ± 0.019(1)	15.568 ± 0.018(1)	15.631 ± 0.018(1)
EGB 1	16.308 ± 0.007(2)	16.439 ± 0.005(2)	16.452 ± 0.007(2)	16.482 ± 0.022(2)
EGB 6	15.692 ± 0.002(2)	15.999 ± 0.002(2)	16.137 ± 0.008(2)	16.300 ± 0.009(2)
HaWe 5	17.321 ± 0.014(2)	17.439 ± 0.005(2)	17.471 ± 0.004(2)	17.528 ± 0.011(2)
HDW 3	17.084 ± 0.003(3)	17.187 ± 0.004(3)	17.218 ± 0.039(3)	17.234 ± 0.019(3)
HDW 4	16.310 ± 0.011(1)	16.540 ± 0.013(1)	16.638 ± 0.017(1)	16.739 ± 0.017(1)
IsWe 1	16.374 ± 0.017(3)	16.523 ± 0.007(3)	16.576 ± 0.016(3)	16.644 ± 0.013(3)
IsWe 2	18.142 ± 0.026(5)	18.160 ± 0.033(5)	18.118 ± 0.026(5)	18.098 ± 0.022(5)
JnEr 1	16.775 ± 0.005(2)	17.128 ± 0.013(2)	17.288 ± 0.001(2)	17.501 ± 0.023(2)
K 1-13	18.051 ± 0.013(3)	18.425 ± 0.006(3)	18.592 ± 0.019(3)	18.846 ± 0.044(3)
K 2-2	13.977 ± 0.007(3)	14.263 ± 0.010(3)	14.390 ± 0.008(3)	14.553 ± 0.013(3)
NGC 3587	15.414 ± 0.001(3)	15.777 ± 0.009(3)	15.960 ± 0.006(3)	16.194 ± 0.029(3)
NGC 6720	15.405 ± 0.016(2)	15.769 ± 0.023(2)	15.901 ± 0.003(2)	16.062 ± 0.012(2)
NGC 6853	13.749 ± 0.026(3)	14.089 ± 0.010(3)	14.247 ± 0.006(3)	14.405 ± 0.010(3)
PuWe 1	15.291 ± 0.008(2)	15.545 ± 0.006(2)	15.662 ± 0.011(2)	15.792 ± 0.008(2)
Sh 2-78	17.633 ± 0.012(2)	17.660 ± 0.005(2)	17.608 ± 0.025(2)	17.543 ± 0.027(2)
Sh 2-176	18.489 ± 0.086(3)	18.559 ± 0.019(3)	18.570 ± 0.016(3)	18.545 ± 0.029(3)
Sh 2-176[a]	18.442 ± 0.018(2)	18.551 ± 0.016(2)	18.562 ± 0.009(2)	18.531 ± 0.010(2)
Sh 2-188	17.424 ± 0.013(3)	17.447 ± 0.004(3)	17.398 ± 0.009(3)	17.376 ± 0.011(3)
Ton 320	15.379 ± 0.007(2)	15.725 ± 0.006(2)	15.890 ± 0.010(2)	16.105 ± 0.018(2)
WeDe 1	16.958 ± 0.007(3)	17.226 ± 0.004(3)	17.338 ± 0.010(3)	17.489 ± 0.016(3)

[a]These measurements are obtained by excluding the observations taken on night 3.

Table 7. Bandpass central wavelengths after convolution with a 100 kK, log $g = 7$, solar abundance synthetic stellar atmosphere and resulting extinctions according to Cardelli et al. (1989).

Band	λ_0	$A_\lambda/E(B-V)$
U	3597 Å	4.86
B	4386 Å	4.12
V	5491 Å	3.10
R	6500 Å	2.10
I	7884 Å	1.90
J	1.237 μm	0.889
H	1.645 μm	0.562
K	2.212 μm	0.349
J_{2MASS}	1.241 μm	0.885
H_{2MASS}	1.651 μm	0.349
K_{2MASS}	2.165 μm	0.361

final results. The bandpass central wavelengths thus determined and the values of the wavelength-specific extinctions are presented in Table 7.

The $V - I$ or $V - J$ observed dereddened colours are then compared with the predicted ones so as to determine if a flux excess exists. An *I* (*J*)-band excess is detected every time the observed (dereddened) and predicted colours are different by more than the combined uncertainties. While a high-confidence result can already lend substantial weight towards a binary interpretation, a lower sigma result needs to be confirmed by additional photometry or spectroscopy.

To predict the $B - V$, $V - I$, $V - J$, $R - I$ and $J - H$ colours of single post-AGB stars, we use theoretical stellar atmosphere models calculated with the simulation code TMAW, the web interface to TMAP (Werner & Dreizler 1999; Rauch & Deetjen 2003; Werner et al. 2003), or the German Astrophysical Virtual Observatory grid calculations TheoSSA.[2] The colours and further details of the calculations are provided in Appendix B (Table B1).

The uncertainties on the measurements (see Section 4.1) are combined with the uncertainty on the predicted colours to derive an uncertainty on the colour excess. The uncertainty on the theoretical colours reflects solely the uncertainty on the temperature. We assume that additional sources of uncertainty are far smaller and do not play a role. The uncertainty on colours derived from the uncertainty on the temperature is quite small, in particular for stars hotter than ∼50 kK, which is the case for most of our sample. Systematic uncertainties on the theoretical, single-star colours are estimated to be below 1 per cent (e.g. Rauch et al.

[2] dc.zah.uni-heidelberg.de/theossa/

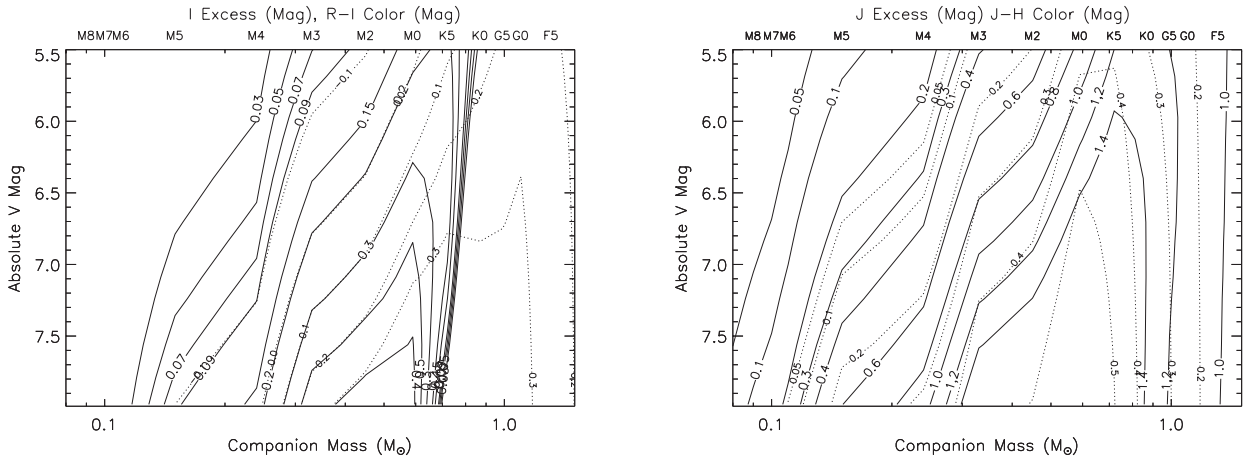

Figure 2. The *I*- and *J*-band excess (solid contours) and $I - R$ and $J - H$ colours (dotted contours) that are produced by main-sequence companions (M9V to F5V) as a function of companion mass and primary's absolute *V* magnitude. These plots are obtained by assuming that the central stars are on the cooling-curve part of the Herzsprung-Russell diagram and cannot be used to determine the spectral type of the companion of objects which have not yet turned the 'knee' on the post-AGB evolutionary track. The *I*- and *J*-band excess correspond to the $\Delta(V - I)$ and $\Delta(V - J)$ listed in Tables 8 and 9.

2007). In fact, the observational uncertainties dominate the error budget.

To further exemplify the technique, we present in Fig. 2 the predicted *I*- and *J*-band excess as a function of primary star absolute *V* magnitude (M_V) and main-sequence companion mass/spectral type. This plot gives a good idea of the ability of the *I*- and *J*-band methods to detect companions, although it must be pointed out that this figure is only valid for those stars that have already entered the cooling track. To generate Fig. 2, we created a grid of M_V absolute stellar brightness for the hot central stars using the effective temperatures to determine both bolometric luminosities and bolometric corrections. The former was determined using the average of the cooling track temperature–luminosity relations of Schönberner (1993), Vassiliadis & Wood (1994) and Blöcker (1995) (for a 1.5-$M_\odot$ main-sequence star, but the scatter is very small). The latter was determined using the average of the relation determined by Vacca, Garmany & Shull (1996) and a blackbody curve. To each hot central star we added the flux of a range of main-sequence companions using magnitudes and colours reported in Appendix C. We thus created a grid of binaries. Next, we calculated the total (binary) $B - V$ colour for each primary–secondary combination and compared it to that of the primary alone. A difference is only present when the companion contributes flux in the *V* or even *B* and *V* bands, which is the case for companions brighter than K0–5V. Any difference is interpreted as reddening and used to deredden all bands. We then subtract the primary *I*-band flux from the binary (dereddened) one and any difference is labelled as excess (this is the value reported on each contour line).

As can be seen in Fig. 2, a measured *I*- or *J*-band excess corresponds to two distinct companion spectral types. This is due to the contribution of the brightest companions to the *V* and even *B* bands, resulting in too high a predicted reddening, too blue a dereddened spectral energy distribution (SED) and therefore smaller *I*- or *J*-band excess. This effect is less pronounced for the *J* band, because reddening effects are smaller in that band. The $R - I$ colour provides an approximate way to distinguish between the two companion spectral types allowed by a given *I*-band excess, while the $J - H$ colour is not as discriminating (see the dashed contours in Fig. 2).

In actuality, we do not rely on the diagrams in Fig. 2 to determine the companions' spectral types and their limits. Rather, we predict the primary's *I* (*J*)-band absolute magnitude using the distance (Table 1), and together with the observed one we derived the secondary's absolute *I* (*J*) magnitude, which we then convert into a spectral type using the table in Appendix C. In this way we do not rely on the $T_{\rm eff}-M_V$ relation characteristic of a given cooling curve. However, the companion spectral types listed in Tables 8 and 9 are consistent with those that would be derived using Fig. 2 within one spectral subtype, except for the two objects with companions brighter than the spectral type K0V, of which we speak more in Sections 8.4 and 8.6.

6 RESULTS

Those objects for which $\Delta(V - I) > \sigma_{\Delta(V-I)}$ [or, equivalently, $\Delta(V - J) > \sigma_{\Delta(V-J)}$] are considered as cases where a companion is detected. We note that this difference is the same as what we call the *I* (*J*)-band excess in Fig. 2, because the theoretical colours are normalized to the observed (dereddened) *V* magnitudes. Reddenings, intrinsic $V - I$ ($V - J$) and $R - I$ ($J - H$) colours, *I* (*J*)-band excesses ($\Delta(V - I)$ or $\Delta(V - J)$), companions' absolute *I* (*J*)-band magnitudes and companions' spectral types are listed in Tables 8 (9). The *I* (*J*)-band excesses are plotted as a function of stellar temperature in Fig. 3 (4).

The reddenings derived by comparing observed and (single-star) predicted $B - V$ colours are compared to those derived from nebular methods in Fig. 5. Most reddenings compare well. The five exceptions are A57 and A79, whose high derived stellar reddenings are likely due to bright companions affecting the *B* and *V* bands, A71, EGB 1 and Sh 2-78, for which we suspect that the nebular reddenings have uncertain values.

We have nine detections or marginal detections in the *I* band: A16 (at the 2σ level), A57 (at the 1.9σ level), A79 (at the 1.5σ level), A84 (at the 1.2σ level), EGB 1 (at the 1.2σ level), HDW 4 (at the 1σ level, but this is a PN mimic), Sh 2-78 (at the 1.7σ level), Sh 2-176 (at the 1.2σ level, only for the measurement excluding night 3) and Sh 2-188 (at the 1σ level). A79 was already known to have an F0V companion (Rodríguez et al. 2001). The spectral type determined with our method is cooler because the reddening was overestimated due to the strong contribution of the companion in the *V* band (see Section 5). We have therefore 8 detections out of 27 *bona fide* objects.

Table 8. *I*-band excesses ($\Delta\,(V-I)$), companion absolute *I*-band magnitudes (M_{I2}) and spectral types (or limits) of our targets.

Name	$E(B-V)$	$(V-I)_0$	$(R-I)_0$	$\Delta(V-I)$	M_{I2}	Comp. spec. type
A7	0.02 ± 0.02	-0.35 ± 0.08	-0.19 ± 0.06	-0.01 ± 0.08	>9.60	Later than M4V
A16	0.13 ± 0.03	-0.12 ± 0.11	0.02 ± 0.09	0.22 ± 0.11	8.30 [9.24–7.73]	M3V [M3V–M1V]
A20	0.07 ± 0.02	-0.32 ± 0.08	-0.16 ± 0.06	0.02 ± 0.08	>7.29	Later than M0V
A28	0.02 ± 0.07	-0.35 ± 0.24	-0.19 ± 0.18	-0.02 ± 0.24	>8.18	Later than M2V
A31	0.00 ± 0.02	-0.29 ± 0.08	-0.14 ± 0.06	0.06 ± 0.08	>9.14	Later than M3V
A57	0.46 ± 0.04	-0.03 ± 0.15	0.15 ± 0.12	0.29 ± 0.15	5.51 [6.56–4.79]	K3V [K7V–G8V]
A71	0.38 ± 0.02	-0.31 ± 0.08	-0.01 ± 0.07	0.05 ± 0.08	>10.56	Later than M5V
A72	0.04 ± 0.04	-0.35 ± 0.14	-0.15 ± 0.14	0.01 ± 0.14	>6.84	Later than K8V
A79	1.20 ± 0.01	-0.21 ± 0.10	0.42 ± 0.10	0.15 ± 0.10	3.12 [4.44–2.66]	F6V [G6V–F3V]
A84	0.11 ± 0.03	-0.22 ± 0.10	-0.08 ± 0.08	0.12 ± 0.10	10.00 [11.91–9.28]	M4V [M6V–M3V]
DeHt 5	0.07 ± 0.03	-0.22 ± 0.11	-0.08 ± 0.09	0.10 ± 0.11	>9.28	Later than M3V
EGB 1	0.20 ± 0.01	-0.29 ± 0.06	-0.07 ± 0.05	0.07 ± 0.06	10.05 [11.96–8.91]	M4V [M6V–M3V]
EGB 6	0.03 ± 0.01	-0.34 ± 0.03	-0.17 ± 0.03	0.01 ± 0.03	>9.79	Later than M4V
HaWe 5	0.14 ± 0.03	-0.25 ± 0.10	-0.08 ± 0.08	0.06 ± 0.10	>11.21	Later than M5V
HDW 3	0.23 ± 0.01	-0.32 ± 0.04	-0.06 ± 0.05	0.03 ± 0.04	>10.35	Later than M4V
HDW 4	0.04 ± 0.02	-0.24 ± 0.07	-0.11 ± 0.06	0.07 ± 0.07	13.05 [16.87–12.30]	M7V [M8V–M6V]
IsWe 1	0.19 ± 0.03	-0.35 ± 0.09	-0.11 ± 0.08	0.01 ± 0.10	>9.77	Later than M4V
IsWe 2	0.32 ± 0.04	-0.32 ± 0.16	-0.04 ± 0.12	0.04 ± 0.16	>9.38	Later than M4V
JnEr 1	0.00 ± 0.01	-0.37 ± 0.06	-0.21 ± 0.05	-0.01 ± 0.06	>10.86	Later than M5V
K 1-13	0.00 ± 0.07	-0.42 ± 0.24	-0.25 ± 0.19	-0.09 ± 0.24	>8.85	Later than M3V
K 2-2	0.02 ± 0.02	-0.31 ± 0.09	-0.17 ± 0.07	0.01 ± 0.09	>7.40	Later than M1V
NGC 3587	0.00 ± 0.04	-0.42 ± 0.15	-0.23 ± 0.12	-0.07 ± 0.15	>8.96	Later than M3V
NGC 6720	0.00 ± 0.03	-0.29 ± 0.11	-0.16 ± 0.08	0.06 ± 0.11	>7.99	Later than M2V
NGC 6853	0.00 ± 0.03	-0.32 ± 0.11	-0.16 ± 0.08	0.04 ± 0.11	>8.42	Later than M3V
PuWe 1	0.08 ± 0.02	-0.34 ± 0.09	-0.14 ± 0.07	0.01 ± 0.09	>10.46	Later than M4V
Sh 2-78	0.31 ± 0.01	-0.26 ± 0.06	0.00 ± 0.06	0.10 ± 0.06	10.22 [11.32–9.72]	M4V [M5V–M4V]
Sh 2-176	0.26 ± 0.09	-0.30 ± 0.32	-0.03 ± 0.25	0.05 ± 0.32	>8.91	Later than M3
Sh 2-176[a]	0.23 ± 0.02	-0.25 ± 0.09	-0.01 ± 0.07	0.11 ± 0.09	10.68 [12.87–9.95]	M5V [M6V–M4V]
Sh 2-188	0.31 ± 0.01	-0.30 ± 0.05	-0.04 ± 0.04	0.05 ± 0.05	10.46 [14.33–9.71]	M4V [M8V–M4V]
Ton 320	0.00 ± 0.04	-0.38 ± 0.14	-0.21 ± 0.11	-0.05 ± 0.14	>9.24	Later than M3V
WeDe 1	0.06 ± 0.01	-0.34 ± 0.03	-0.16 ± 0.03	0.01 ± 0.03	>11.36	Later than M5V

[a]These measurements are obtained by excluding the observations taken on night 3.

Table 9. *J*-band excesses ($\Delta\,(V-J)$), companion absolute *J*-band magnitudes (M_{J2}) and companion spectral types (or limits) of our targets. All detections and limits are consistent with the results of the *I*-band excess (Table 8).

Name	$E(B-V)$	$(V-J)_0$	$(J-H)_0$	$\Delta(V-J)$	M_{J2}	Comp. spec. type
A7	0.02 ± 0.02	-0.66 ± 0.11	-0.07 ± 0.20	0.15 ± 0.11	9.65 [11.07–8.95]	M5V [M8V–M5V]
A31	0.00 ± 0.02	-0.41 ± 0.07	0.15 ± 0.03	0.40 ± 0.07	8.26 [8.57–7.98]	M4V [M4V–M4V]
A72	0.04 ± 0.04	-0.68 ± 0.17	–	0.16 ± 0.17	>6.57	Later than M1
A79	1.20 ± 0.01	-0.74 ± 0.06	0.02 ± 0.07	0.10 ± 0.06	4.05 [5.17–3.45]	G7V [K5V–G1V]
DeHt 5	0.07 ± 0.03	-0.24 ± 0.14	–	0.54 ± 0.14	8.80 [9.30–8.37]	M5V [M5V–M4V]
EGB 1	0.20 ± 0.01	-0.65 ± 0.11	–	0.18 ± 0.11	9.43 [10.52–8.80]	M5V [M6V–M5V]
EGB 6	0.03 ± 0.01	-0.54 ± 0.09	0.38 ± 0.10	0.28 ± 0.09	9.15 [9.67–8.76]	M5V [M5V–M5V]
K 2-2	0.02 ± 0.02	-0.71 ± 0.09	-0.06 ± 0.08	0.01 ± 0.09	>7.84	Later than M4V
NGC 3587	0.00 ± 0.04	-0.93 ± 0.18	–	-0.12 ± 0.18	>10.12	Later than M6V
NGC 6720	0.00 ± 0.03	-0.63 ± 0.22	–	0.19 ± 0.22	>7.97	Later than M4V
NGC 6853	0.00 ± 0.03	-0.66 ± 0.11	0.05 ± 0.06	0.17 ± 0.11	8.81 [10.05–8.12]	M5V [M6V–M4V]
Ton 320	0.00 ± 0.04	-0.87 ± 0.20	–	-0.08 ± 0.20	>9.92	Later than M6V

In the *J* band we detected A7 (at the 1.4σ level), A31 (at the 4.7σ level), A79 (at the 1.7σ level), DeHt 5 (at the 3.8σ level, but this is a PN mimic), EGB 1 (at the 1.6σ level), EGB 6 (at the 3.1σ level) and NGC 6853 (at the 1.5σ level). We have therefore 6 detections out of 11 *bona fide* central stars with data.

The spectral types of the companions implied by the detected excesses as well as limits of the non-detections are also listed in Tables 8 and 9. When a companion was not detected, we summed the *I* (*J*)-band excess with the upper error bars to create an upper limit to the flux excess and determined an upper limit for the companion mass/spectral type in this way. We note that all limits and detections are fully consistent across the two detection techniques.

The *I*-band binary fraction is determined by the ratio of 8 objects over 27 *bona fide* central stars (see Section 2 for an explanation of what we mean by *bona fide*), or 30 per cent. Only companions brighter than the spectral type M3–4V can be detected by our survey, where this limit was estimated by taking the median of the limits in Table 8. Within the *J*-band group, the detection rate is 6 out of 11, or 54 per cent, in line with the study of Frew & Parker (2007, see also Frew 2008). A look at Table 9 shows that most detections in the *J* band were fainter, in line with the expectation that the *J* band is a

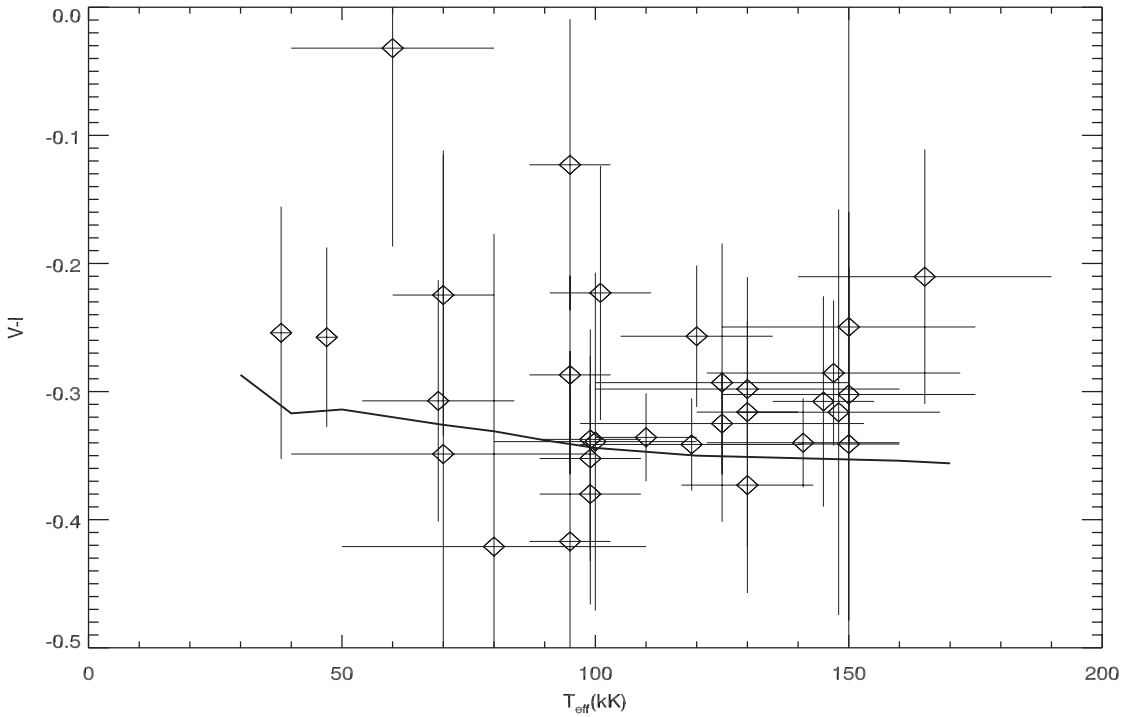

Figure 3. The observed (dereddened) $V - I$ colours of our targets (symbols; see Table 8) compared with the predicted $V - I$ colours of single stars as a function of the effective temperature (for $\log g = 7.0$ – solid line).

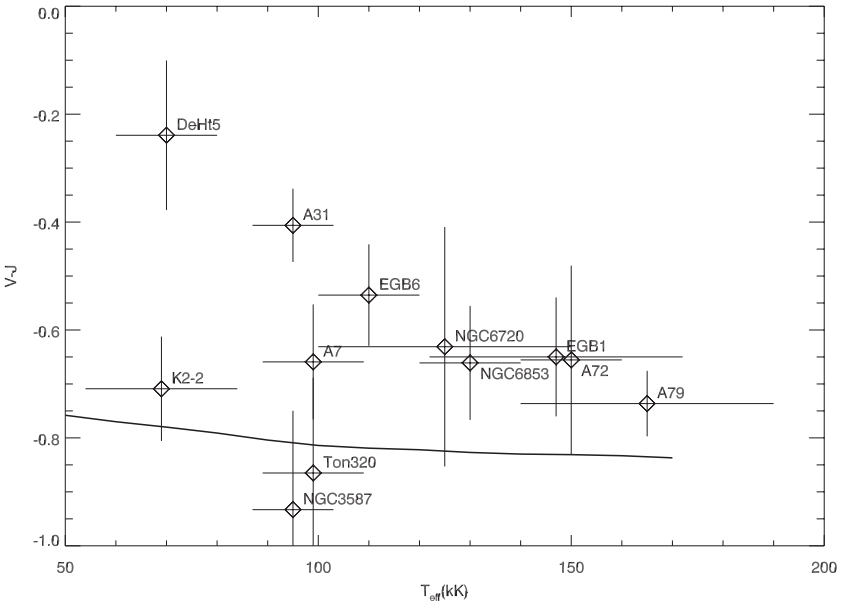

Figure 4. The observed (dereddened) $V - J$ colours of our targets (symbols; see Table 9) compared with the predicted $V - J$ colours of stars as a function of the effective temperature (for $\log g = 7.0$).

more sensitive method. Based on the detection and limits of Table 9 we guesstimate that this limit is M5–6V. The binary fraction for the entire sample, obtained from either the *I*- or *J*-band excess method, is 44 per cent (12 out of 27 bona fide PN) to a limit intermediate between the two methods.

Before comparing our results with predictions, we would like to remark on the asymmetry of the distribution of $V - I$ colours of our sample about the single-star prediction line (Fig. 3). Even eliminating from that plot the nine detections, which are all above the prediction, the non-detections (21 objects) still preferentially lie above the single-star prediction line (15 versus 6 objects). We speculate that this points to the detection of a binary signal which is higher than the fraction we determined from individual objects above. To determine whether this is significant we would need a Monte Carlo simulation. One could counterargue that this asymmetry is caused by an incorrect placement of the prediction line or, in other words, that the predicted colours are too blue. Shifting the prediction line so that the non-detected data points scatter

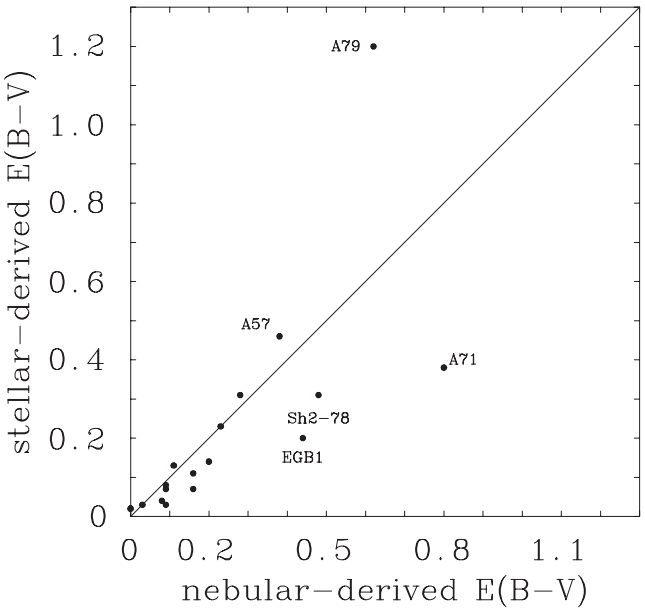

Figure 5. A comparison of the reddening values obtained via a nebular method (Table 1) and those obtained via our stellar method (Table 8).

symmetrically about it would require a systematic shift of the synthetic $V - I$ colours of about ∼5 per cent which is excluded by the comparison of synthetic spectra with data carried out over the years (Rauch, private communication; Rauch et al. 2007).

Finally, we have demonstrated that the *I*-band excess method necessitates extraordinary accuracy, such as that achieved for the current data set, but is not usually encountered in unvetted data from the literature. For example, in Fig. 6 we compare the *I*-band excesses obtained by using the *B*, *V* and *I* data compilation of Bilíková et al. (2012) with our data set. Using all of their data and determining the stellar temperatures in the same way as we have done for our sample, we see how the scatter around the single-star prediction is dramatic. While their compilation was not aimed at detecting binarity, it can easily be seen that data from the literature are not generally suitable for this type of work.

6.1 Photometric variability

Periodic variability in central stars of PN usually denotes a short-period binary (e.g. Miszalski et al. 2009). Variability should not interfere with the detection of an IR excess because the exposures in each filter are taken in a short sequence and the periods of these objects are of the order of 12 h (De Marco, Farihi & Nordhaus 2009). Although it is expected that the colour of the short-period binary should vary during the orbit, this is only marginally so (e.g. De Marco et al. 2008). Variability can however increase the error on the absolute photometry because we average observations taken at more than one epoch. We have therefore monitored all targets for variability during photometric as well as non-photometric nights. The differential magnitudes to five field stars are then plotted as a function of time. The central stars for which the scatter of the average differential magnitudes in each filter is larger than the mean errors on these magnitudes are labelled as possible variables. Further, we retain as likely variables those of the stars for which the variability trends are the same in all filters. We will continue monitoring these stars to determine if a period is present. The variable stars are A57, A72, A84, IsWe 2, Sh 2-78 and Sh 2-176. Four of the six variables have an *I*-band excess, as one might expect if the variability denotes binarity. Further comments on the variables are reported in Section 8.

7 COMPARISON OF THE OVERALL PN BINARY FRACTION WITH THE OVERALL MAIN-SEQUENCE BINARY FRACTION

We recognize that the binary fraction determined here is preliminary because of the small sample size. However, here we compare it with the prediction from the current PN evolution scenario, whereby PN derive from *all* ∼1- to 8-$M_\odot$ stars, whether they are single stars or are in binaries. As already explained, it is this prediction that we are testing. We expect that if PN derive from a binary interaction more often than for the current evolutionary scenario, we would find a larger fraction of short- and intermediate-period binaries in the central star population. This leads to the prediction that the *overall* binary fraction, i.e. where we consider binaries at any period, should also be larger in the *binary hypothesis* than in the standard scenario.

The progenitor population of the PN from which we have drawn our targets is the main-sequence stars with masses between ∼0.9 and 8 $M_\odot$. We can then use the main-sequence population binary

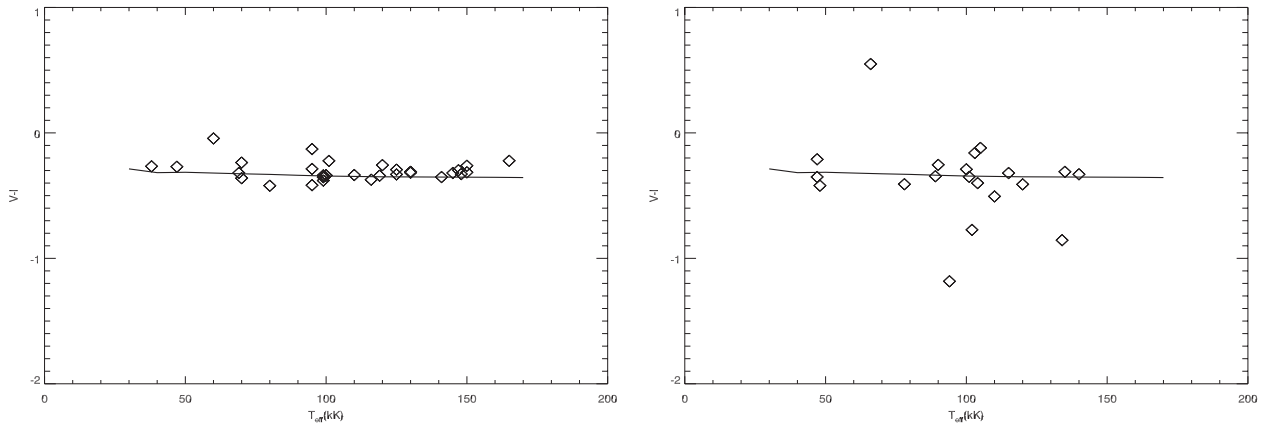

Figure 6. Left-hand panel: the same figure as Fig. 3, except that here we compare our results (with no error bars, for clarity) with results obtained using the data compiled by Bilíková et al. (2012, right-hand panel), showing how unvetted data have much larger random errors.

fraction of Raghavan et al. (2010) to represent the binary fraction of the progenitor population of our PN. We use (50 ± 4) per cent, which is the percentage of double and multiple star systems with primaries in the spectral type range F6V–G2V (masses in the range 1.27–1.03 $M_\odot$; see Table C1). This is reasonable on the grounds that the median progenitor mass of today's PN is 1.2 $M_\odot$ (Moe & De Marco 2006). This fraction is lower than that determined by Duquennoy & Mayor (1991, 57 per cent) who accounted for a larger incompletion bias, but is likely to be more accurate. This fraction includes *any main-sequence companion down to the planetary regime at any separation*.

7.1 Accounting for completion effects

Before we can carry out a comparison we need to increase the PN binary fraction to (i) include the companions that have not been detected because they are too faint; (ii) include wide companions, because our observed sample does not contain resolved binaries by design. Finally, we need to (iii) account for the fact that some main-sequence close binaries go through a common envelope interaction on the RGB. Those systems will become short-period binaries with very low mass envelopes (the primary will become a subdwarf O or B star; Morales-Rueda et al. 2003) and are unlikely to ever ascend the AGB on the grounds of low envelope masses (Dorman, Rood & O'Connell 1993); if they do, they will suffer a second common envelope almost immediately which would result in a subluminous object, highly unlikely to ever make a visible PN.

(i) To account for companions with an M3–4V spectral type or fainter (mass $\leq$0.33–0.24 $M_\odot$), we use table 18 of Raghavan et al. (2010) that lists all the companion spectral types of the detected binaries. We determine that the fraction of main-sequence binaries with a companion spectral type of M3–4V or later is 41–31 per cent (73–56 of 179 main-sequence binaries for which the companion spectral type is known, where we count as undetectable also 4 hot and evolved companions). We therefore increase our *I*-band-derived PN binary fraction (30 per cent) by a factor of 1.69–1.45 to account for the undetected faint companions.
To account instead for companions with brightness equal to or fainter than M5–6V (the limit we estimated for the *J*-band data set), we would have to multiply the *J*-band-derived PN binary fraction (54 per cent) by a factor of 1.28–1.19.

(ii) The ground-based spatial resolution of our observations is probably only slightly smaller than the median seeing of 1.3 arcsec corresponding to a projected separation of ∼1040 au for the median distance of our sample of 0.80 pc. To deproject this separation we would have to divide the projected separation by a factor of 0.8, which accounts for the systems' random phase *and* random orientation. However, if we also account for an eccentricity distribution similar to the main sequence's, this factor approaches unity, because systems spend more time near apastron in eccentric systems. Not knowing the eccentricity distribution of central star binaries but presuming a degree of circularization to have taken place, we deproject the projected separation using a range of factors (0.8–1.0). The median separation is then converted to a period in the range ∼13 000–18 000 yr ($\log(P/\mathrm{d}) = 7.11$–$7.25$), using Kepler's third law and a total system mass of 0.9 $M_\odot$. This period limit is then decreased to $\log(P/\mathrm{d}) = 6.71-6.85$, to account for the fact that, due to mass-loss and angular momentum conservation, the orbit of a typical binary will widen by a factor of 2–3 (we used 2.5) and so some of the main-sequence binaries of Raghavan et al. (2010) will become resolved central star binaries in our sample because of orbit widening.

A similar argument can be applied to the *J*-band sample of 11 bona fide PN, which have a median distance of 0.65 kpc, with a resulting median projected separation of 845 au, resulting in a period corrected for orbit widening of $\log(P/\mathrm{d}) = 6.57-6.71$.

(iii) Finally, the main-sequence binary population with period shorter than $\log(P/\mathrm{d}) = 2.43$ never ascends the AGB. This value was calculated using a radius on the RGB of 100 $R_\odot$ [see, e.g., fig. 5 of De Marco et al. (2011)] and a maximum tidal capture radius of 2 stellar radii (using a total system mass of 1.5 $M_\odot$). The maximum tidal capture radius for the RGB was obtained from Villaver & Livio (2009) and Madappatt et al. (2011). At this point we integrate under the normalized main-sequence binary period distribution of Raghavan et al. (2010, their fig. 13) using $\log(P/\mathrm{d}) = 2.43$–$6.78$ as limits (or 2.43–6.65 for the *J*-band sample; where we have taken the average of the period separation ranges to determine the upper limits), obtaining a fraction of 0.65 of the total (or 0.64, for the *J*-band sample): these are the systems we detect. This translates into a second factor of 1.54 (or 1.56), which we multiply by the central star binary fraction so as to include binaries at all separations and thus make it comparable to the main-sequence one.

(iv) The only bias that is impossible to account for is that due to central stars whose companions are bright enough to contribute to the *V* and even *B* bands. As we have explained in Section 5, these will result in reddenings that are artificially large, because the bright companions tend to make their system's colours redder. Once this overlarge reddening is applied to all the bands, the binary SED is rendered bluer than it should be and the *I*- or *J*-band excess is necessarily reduced. The mismatch between the reddening curve and SED of the companion can decrease the red/IR flux excess below detectability or reduce it such that it is impossible to match it to a companion spectral type. Interestingly, only six objects have stellar-derived reddening values that are larger than the nebular-derived values, the most noticeable being A79, a known binary and A57 which has a large *I*-band excess. For the other four objects (A7, A16, A28 and Sh 2-188), these discrepancies are however always within the uncertainties. We therefore conclude that either the reddening comparison is not reliable due to high errors in nebular-derived reddenings or that our sample does not tend to include companions much hotter than the spectral type K0V. This makes sense in view of the fact that only a minority of companions are expected to be that hot. We leave this bias unquantified in the knowledge that it would be at most a few per cent. A spectroscopic follow-up will resolve this issue.

7.2 The debiased PN binary fraction and its uncertainties

The debiased central star binary fraction obtained through the *I*-band photometry of our sample is 67–78 per cent. Using the *J*-band data alone we obtain a fraction of 100–107 per cent. The ranges account for the uncertainty on the factor to account for the unobservable faint companions. The error bars on these estimates are difficult to estimate for the moment and we defer this exercise to the next paper in this series, which will increase the sample. However, if all limits were accurately accounted for, then the *I*- and *J*-band fractions should be the same. We therefore tentatively estimate a 10–30 per cent error bar. We preliminarily conclude that the PN binary fraction is higher than the main-sequence binary fraction of (50 ± 4) per cent.

We can also estimate the PN binary fraction after eliminating from each of the *I* and *J* samples the one detection with the smallest

statistical relevance. By doing so, we would obtain *I* and *J* binary fractions of 58–68 and 84–90 per cent, respectively.

7.3 Comparison of the short-period PN binary fraction with the main-sequence binary fraction

The fraction of PN that surround short-period, post-common envelope binaries is 15–20 per cent (Bond 2000; Miszalski et al. 2009). This is a very large fraction when we consider that only a very small minority of main-sequence binaries would suffer a common envelope on the AGB.

The fraction of main-sequence binaries that go through a common envelope on the AGB, resulting in post-common envelope central stars of PN, should be quite small: only those companions that escape capture on the RGB, but then are successfully captured on the AGB, will become post-common envelope central stars. These are companions that, while on the main sequence, have periods in the range $\log(P/\mathrm{d}) > 2.7-2.8$ and therefore account for only $\sim$1 per cent of all main-sequence binaries. The lower period limit was calculated in Section 7, while the higher period limit was obtained by considering that for a successful AGB capture the orbital separation has to be smaller than approximately twice the maximum AGB radius (Villaver & Livio 2009; Nordhaus et al. 2010; Madappatt et al. 2011). The maximum AGB stellar radius for a 1.2-$M_\odot$ star was calculated to be $\sim$300 $R_\odot$ (De Marco et al. 2011, with the usual adjustment for the orbital widening due to mass-loss, see Section 7). Even exaggerating the maximum AGB radius (600 $R_\odot$) and the maximum capture radius to 5 stellar radii, we get $\log(P/\mathrm{d}) = 3.9$ and a fraction of 5 per cent. We would therefore predict a similar fraction of post-common envelope central stars, contrary to the observations.

7.4 Comparison of the PN binary fraction with the white dwarf binary fraction

We note, finally, that the PN binary fraction, even before detection biases are accounted for, appears to be higher than the white dwarf binary fraction of 25 per cent (Holberg 2009, the WD binary fraction should be a few points higher, if we could readily detect white dwarfs around bright main-sequence stars – Sirius-like systems). One reason could be that the white dwarfs derive from a population that includes lower mass stars, those that do not develop a PN due to long transition times. Such lower mass population would naturally have a lower binary fraction (Raghavan et al. 2010). Another reason could be that PN form preferentially around binaries, the hypothesis we are trying to test. To discern between the two explanations of the discrepancy between the white dwarf and PN binary fractions, we need better constraints on white dwarfs and central stars masses (Liu et al. 1995; Liebert, Bergeron & Holberg 2005; Gesicki & Zijlstra 2007).

8 NOTES ON REMARKABLE INDIVIDUAL OBJECTS

8.1 Abell 7

This star was detected in the *J* band (at the 1.4σ level) and the implied companion would be an M5V star. Companions dimmer than M4V are excluded by the *I*-band photometry. The central star has a red dwarf companion 0.91 arcsec away from the central star (Ciardullo et al. 1999) resolved by the *Hubble Space Telescope* (*HST*), which warrants further investigation in order to determine a photometric parallax; only an upper limit of K2V could be determined from the *HST* data of Ciardullo et al. (1999), while Frew (2008) determined a spectral type of M4V, similar to our own.

8.2 Abell 16

We detected an M3V companion in the *I* band at the 2σ level.

8.3 Abell 31

Ciardullo et al. (1999) give an upper limit to the distance of 440 pc (based on photometry of the resolved companion), mildly inconsistent within the uncertainties with a direct trigonometric determination of $D = 568^{+131}_{-90}$ pc (Harris et al. 2007). Our *I* and *J* photometry suggest an M4V companion, in agreement with Frew (2008) and Ciardullo et al. (1999), who used the *HST* to determine a separation of 0.26 arcsec for a companion with spectral type later than M4V. This companion may never have interacted with this PN. The morphology of this PN is likely round, in agreement with the lack of interaction.

8.4 Abell 57

The *I*-band excess detected for this object exceeds the uncertainty by a factor of 2 and the spectral type of the companion is K3V. Such a bright companion may have contributed in the *V* band. In fact, the reddening derived from our method is higher than the reddening derived from nebular observations (cf. Tables 1 and 6). We also note that we used the limiting temperature of 60kK for this star. A higher temperature would lower the *I*-band excess slightly, with a temperature of 150kK, reducing it to 0.25 mag. Miszalski et al. (2011) discovered this to be another example of an EGB 6-like central star (Frew & Parker 2010), implying the presence of a compact disc either around the central star or its companion, lending strong support to this star being a physical binary. This central star appears to be variable at the 0.1-mag level from our differential photometry, while our absolute photometry reveals at most a variability of 2 per cent based on two epochs of data.

8.5 Abell 72

As was the case for A57, the effective temperature of the central star of A72 can be constrained to be larger than 100 kK by the Zanstra method. We therefore adopt a lower limit of 100 kK due to the fact that our own Ultraviolet Visual Echelle Spectrograph spectrum suggests a temperature in excess of 120 kK. There is effectively no difference in the calculated excess for temperatures higher than 100 kK. From *I*- and *J*-band photometry we can state that the companion, if present, would be fainter than the M1V spectral type. We suspect this star to be variable at the 0.05- to 0.1-mag level.

8.6 Abell 79

This star is known to have a cool spectral type (Rodríguez et al. 2001) possibly denoting that it is a binary since the ionizing source of the PN would otherwise be missing. When the cool companion dominates the light of the system, we can assume that it contaminates the *V* or even the *B* band. As a result, the reddening will be too large. We determined $E(B-V) = 1.2$, while a value of 0.62 is derived from near-IR data (Frew 2008). Using our reddening, all the photometry is dereddened excessively, with the resulting derived $V-I$ and $V-J$ colours that are too blue and a reduced *I*- and *J*-band

excess. That is why, the determined companion spectral types (F6V from *I*-band photometry and G7V from *J*-band measurements) are redder/fainter than the one that was determined from spectroscopy (G0V) by Rodríguez et al. (2001). Note how the result from *J*-band photometry is closer to the spectroscopically derived spectral type as predicted in Section 5. In addition, we cannot use the contour plots in Figs 3 and 4 because we do not have the central star's M_V value.

The *I*-band excess for this star is large (0.15 mag) but it is affected by a considerable uncertainty. The reason is that the *I*-band magnitude of this star is 0.2 mag brighter in night 4 than in night 3. While we could exclude the night 3 measurement on the grounds that the night was only partly photometric, our logs show that part of the night was completely clear. In addition, the magnitudes in all other bands are very similar across the two nights. We therefore keep both measurements and accept the large uncertainty.

8.7 Abell 84

The central star of A 84 has a companion detected in the *I* band at the 1.2σ level, making it a marginal detection. The differential photometry shows a clear dimming trend over the eight nights of data at the 0.1-mag level.

8.8 DeHt 5

This large emission nebula (also known as DHW 5) was first identified by Dengel, Hartl & Weinberger (1980) as a likely PN. It has an unusual irregular morphology and shows quite a different appearance in [O III] light, compared to its morphology in [N II] and [S II] emission (Rosado & Moreno 1991; Tweedy & Kwitter 1996). Previous researchers have assumed that DeHt 5 is a bona fide PN. Bannister et al. (2003) had previously noted the proximity of its central star, WD 2218−706, to the giant molecular cloud complex described by Kun (1998) and stated that the star may lie in an area where the ISM is dense. However, these authors did not consider the possibility that the optical nebula might be in fact ionized ISM. Tweedy & Kwitter (1996) also noted the extensive diffuse emission around the bright nebula, suggesting that this might be ionized interstellar material, but assumed that the core was a true PN. Frew (2008) found that the nebular and stellar velocities are different, suggesting that the nebula is unrelated to its ionizing star, a situation similar to PHL 932 (Frew et al. 2010). The overall body of evidence is again in favour of the ionized-ISM interpretation, rather than a PN. The morphology is not typical of an evolved PN, and the gas is consistent with being ionized ambient material, as the systemic velocity agrees with the CO velocities of widespread neutral gas at ∼360 pc, the distance of the star as determined by Benedict et al. (2009). The narrow line width of the nebular gas is also consistent with the ionized-ISM interpretation. Furthermore, the evolutionary position of the star in the Herzsprung-Russell diagram is *not* in agreement with a post-AGB track that is consistent with the time-scale of PN evolution. All of the evidence is consistent with DeHt 5 being an H II region ionized by WD 2218+706. The central star has a detected *J*-band excess, consistent with an M3V companion, but we flag that this is one of two objects with one epoch of measurements only.

8.9 EGB 1

This somewhat irregular, one-sided nebulosity is traditionally classified as a PN. It is poorly studied, but spectra show moderately bright [O III] emission. However, the lack of a limb-brightened bow shock (expected for such a one-sided nebula with an off-centre central star), the small line width (López et al. 2012), the systemic nebular velocity close to zero in the local standard of rest (LSR) and the moderate excitation lead to questions regarding its status. It may be another case of ionized ISM, but more observations need to be obtained before a definitive answer can be given and therefore we have kept it as a PN for the time being. Additionally, the ionizing star is a periodic photometric variable (Hillwig, private communication), consistent with binarity. We detected an *I*- and *J*-band excess at the 1.2σ and 1.6σ levels, respectively, consistent with an M4–5V companion. The hypothesis that the companion to this central star could be a white dwarf is inconsistent with the $R - I$ colour.

8.10 EGB 6

Liebert et al. (1989) found an unresolved, dense emission nebula surrounding the central star, with a tiny ionized mass of $\sim 10^{-9}\,M_\odot$. Zuckerman et al. (1991) found near-IR evidence for a probable red dwarf companion, confirmed by Fulbright & Liebert (1993) via *JHK* photometry of the central star. The companion has been imaged with *HST* (see Bond et al. 1993; Bond 1994) at a projected separation of 0.18 arcsec. Furthermore, the unresolved emission nebula corresponds in position to the red dwarf and not the central star (Bond 1994), suggesting that there may be a small disc of material around the cool companion (possibly accreted from the PN) and photoionized by the central star. This is the archetype of a class of PN central stars with compact, unresolved ionized nebulae (or discs), which Frew & Parker (2010) refer to as EGB 6-like central stars. We detected a 3σ *J*-band excess consistent with an M5V companion, in line with the results of Bond et al. (1993), but we note that the $J - H$ colour is mildly inconsistent with this spectral type, as it appears too red.

8.11 HDW 4

Also designated as HaWe 6, this faint nebula was noted by Hartl, Dengel & Weinberger (1983). Harris et al. (2007) determined a trigonometric distance to the ionizing star of only 209^{+19}_{-16} pc. Napiwotzki (1999) performed an non-local thermodynamic equilibrium (NLTE) model atmosphere analysis, determining $T_{\rm eff} = 47\,300 \pm 1700$ K and $\log g = 7.93 \pm 0.16$, and estimating a distance of 250 pc. The relatively low temperature and high gravity of the white dwarf suggest a long cooling age far greater than any feasible PN lifetime. Referring to table 1 of Bergeron, Wesemael & Beauchamp (1995), a cooling age of 3–4$\times$ 10^6 yr is suggested. The absolute magnitude is $M_V = 9.43^{+0.18}_{-0.19}$ which is considerably fainter than any PN nucleus. The very low ionized mass of the nebula ($5 \times 10^{-3}\,M_\odot$; Napiwotzki 1999) also rules out a PN interpretation. Napiwotzki (1999) speculates that the nebula might be a shell produced by an ancient nova outburst (the mass is approximately right), but the star shows no sign of any cataclysmic variable features in its spectrum (Napiwotzki & Schönberner 1995). Napiwotzki (1999) obtained a spectrum of the H II region around this star and deduced an upper limit to the expansion of $2v_{\rm exp} < 47\,{\rm km\,s^{-1}}$. Hence an expanding nova shell hypothesis is ruled out. The expansion limit is consistent with ambient ISM, so the nebula may be another case of ISM ionization by the unrelated hot white dwarf WD 0533+555 (Frew 2008). We report a very marginal 1σ detection in the *I* band, consistent with an M7V companion. However, this object was observed only once and the observation may have been affected by thin cirrus (Table 3).

8.12 HaWe 5

For the 'central' star, Napiwotzki (1999) determined $T_{\rm eff} = 38\,100 \pm 1500$ K and $\log g = 7.58 \pm 0.20$ from an NLTE model atmosphere analysis. The estimated distance is ∼420 pc. This small faint nebula shares characteristics in common with HDW 4, where the large evolutionary age of the star is greatly at odds with the existence of a remnant PN. Napiwotzki (1999) also suggests that this may be an old nova shell and estimated an ionized mass of only $2 \times 10^{-4}\,{\rm M}_{\odot}$. A red Digitized Sky Survey image shows a vaguely PN-like elliptical nebula surrounding the ionizing star. The small size and faintness of the object would be remarkable if it were a real PN at the nominal distance. Instead, it is more likely to be a wisp of ionized ambient material. We note that the second epoch of this object was suspected non-photometric. The fluxes in the four bands for that exposure were indeed fainter than the other two by 0.03, 0.23 0.15 and 0.01 mag. While clouds are grey and one would expect a similar magnitude drop in all bands, it is possible that the high-cirrus cloud may have changed over the stretch of time over which we took the four exposures. We therefore did not consider the exposures in this epoch for absolute photometry. On the other hand, the other two epochs differed by as much as 0.02 and this may be an indication of intrinsic variability. Our lack of *I*-band detection imposes a limiting companion spectral type of M5V.

8.13 IsWe 2

We are reasonably confident that this star is variable at the 3–4 per cent level, although the clear trend in the *B*, *V* and *R* bands is not clearly evident in the *I* band (Table A1). However, we noted that the *I*-band photometry taken in the second epoch was 30 min later than the other filters, which may have contributed to the lack of a similar trend. From *I*-band photometry we impose a limit of M4V on a companion's spectral type. The error on the average of five epochs is possibly larger than it should be because of the variability.

8.14 K 1-13

This is a faint elliptical/bipolar nebula, also known as Abell 25. The Schlafly & Finkbeiner (2011) asymptotic reddening in this direction is $E(B-V) = 0.03$, so the central star is essentially unreddened. We adopt an integrated Hα flux of $\log F = -11.95$ from Frew, Parker & Boijčić (2012), and Kaler, Shaw & Kwitter (1990) gave an upper limit for the He II $F(\lambda 4686)$ flux of $0.5 \times F({\rm H}\beta)$. Using $V = 18.42$ for the central star, we obtain a hydrogen Zanstra temperature of 49 kK, which is a lower limit. The He II flux limit can be used to derive an upper limit on the temperature of 92 kK for this optically thick PN. We have therefore adopted a temperature of 80 ± 30 kK. We note that Abell (1966) gave $V = 18.94$, $B-V = -0.14$, $U-B = -1.15$, so his *V*-band magnitude is quite different from ours. We impose a limiting spectral type of M3V from *I*-band photometry.

8.15 K 2-2

The ionizing star has a rather low mass (Napiwotzki 1999) and the inferred post-AGB lifetime is not consistent with the kinematic age of the nebula. This object may turn out to be another case of ionized ISM. Like EGB 1, the nebula has a very low line width and a systemic nebular velocity close to zero LSR (López et al. 2012). Alternatively, this PN may be a senile example of a common-envelope ejection event. Afšar & Bond (2005) have suggested that the central star is a likely close binary, based on radial velocity variability. Our *J*-band photometry imposes a limiting spectral type for a companion of M4V.

8.16 NGC 3587

This nebula is also known as M97. The *I*-band magnitude of Ciardullo et al. (1999) is fainter than ours by about one magnitude. We suspect it to be erroneous based on the fact that all available photometry (Sloan Digital Sky Survey, 2MASS and *Spitzer*/Infrared Array Camera) is in line with our *B*, *V* and *I* values. We derive a companion spectral type limit of M6V from *J*-band photometry.

8.17 NGC 6853

This beautiful, bright PN, also known as M 27, is at a distance of $405\ ^{+28}_{-25}$ pc (Benedict et al. 2009). Ciardullo et al. (1999) discuss the companion to the central star discovered by Cudworth (1973). Assuming a physical association, a tentative spectroscopic parallax of 430 pc is derived, in agreement with the trigonometric distance, but a radial velocity measurement for the companion is needed. We detect an M5V companion with *J*-band photometry at the 1.5σ level.

8.18 PuWe 1

The effective temperature of the central star of PuWe 1 was a weighted average of the determination by Napiwotzki (1999), Good et al. (2004) and Gianninas et al. (2010). Harris et al. (2007) give a trigonometric distance of 365^{+47}_{-37} pc. Ciardullo et al. (1999) discuss the nature of a pair of stars (likely a binary) that are located at 5.2 arcsec from PuWe 1's central star. This pair may be a wide companion to the central star, in which case this system would be a triple. However, the proper motion of the pair appears different to that of the central star, which would make the central star not associated with it. Our photometry excludes the optical pair. Our *I* band imposes a limit for a companion spectral type of later than M4V.

8.19 Sh 2-78

This star exhibits variability at the 0.3-mag level over the course of the eight nights. The photometric magnitudes reveal only an ∼0.05-mag brightening between nights 4 and 5. We detected an M4V companion in the *I* band at the 1.7σ level.

8.20 Sh 2-176

This object was detected to be variable at the 5-per cent level from our monitoring data set. Our three epochs of photometric observations reveal that indeed the object brightened between the first two epochs and dimmed thereafter. Although the data in all four filters tell a consistent story, the third epoch data are affected by a larger uncertainty and the *B*-band magnitude is quite a bit dimmer than the other filters. On the grounds of variability and larger errors we excluded the third epoch from the calculation of the average magnitudes (Table 6). By doing so the *I*-band excess is increased and the error is greatly decreased, resulting in a 1.2σ detection of an M5V companion (see the two entries in Table 8).

8.21 Ton 320

The effective temperature of the central star of Ton 320 was determined as the weighted mean of the estimates of Good et al. (2004), Tremblay, Bergeron & Gianninas (2011) and Gianninas et al. (2010), where the gravity was obtained from Gianninas et al. (2010). The ionizing star of this very faint PN (also known as TK 1) has a 2MASS *K*-band excess (Holberg & Magargal 2005) but this

may be spurious since the error bars on that value are large. The most stringent limit on the companion spectral type is imposed by our *J*-band observations (M6V).

8.22 WeDe 1

There is a faint wide companion to the central star of the PN WeDe 1 (also known as WDHS 1; Weinberger et al. 1983), though it is likely to be an optical companion. Our *I*-band photometry cannot detect a companion fainter than the spectral type M5V.

9 CONCLUSIONS AND DISCUSSION

In this work we have started a survey of the 2-kpc, volume-limited sample to determine the binary fraction via a technique able to detect *I*- and *J*-band flux excess due to the presence of a cool companion. For this first survey we have selected 30 central stars of PN, of which we later determined 3 to be PN mimics. Of the remaining 27 central stars we have detected 8 with a possible *I*-band excess (of which one was a previously known binary). For 12 of these objects we collected the best *J*-band photometry from the literature and determined that 6 out of 11 bona fide central stars have a flux excess. In total, we have detected an excess in 11 of the 27 central stars in either or both of the two bands.

For the *I*-band survey we calculate a detected fraction of 30 per cent which, when debiased to account for undetected objects, results in an unbiased binary fraction of 67–78 per cent. There are three principal debiasing factors. The first, to account for the fact that we do not detect companions fainter than M3–4V. The second, to account for the fact that we do not detect wide binaries by design. The third, to account for the fact that main-sequence binaries that go through a common envelope on the RGB do not ascend the AGB and do not become PN. These factors have to be included in order to compare the PN binary fraction with the main-sequence one.

From the *J*-band survey we calculate a binary fraction of 54 per cent which, when debiased to account for binaries at any period and all companions, becomes 100–107 per cent, clearly showing that the error bar due to the low-number statistics is high. The discrepancy between the *I*- and *J*-band fractions is likely an effect of the low-number statistics. Since the binary fraction determined using *I*-band photometry relies on more data than using the *J*-band photometry, it is likely that the *I*-band fraction is more accurate (even if the *I* band is less sensitive). However, the *J*-band fraction agrees with the preliminary work of Frew & Parker (2007), who used 34 objects (although their detection limits were poorly quantified).

Thus debiased we can compare these fractions with that of F6V–G2V main-sequence star binaries of (50 ± 4) per cent (Raghavan et al. 2010). We preliminarily conclude that there may be an overabundance of central star binaries, compared to the putative parent population.

We have also noticed how, starting from the main-sequence binary fraction and period distribution, we would expect only a few per cent of central stars of PN to be post-common envelope binaries, whereas previous surveys detected 15–20 per cent. This discrepancy can only be reconciled within the *binary hypothesis*.

Here we have demonstrated that the binary fraction is an elusive quantity. Even the best, most accurate observations cannot easily detect faint companions and the only way to reduce the error is by analysing a much larger sample with similarly accurate photometry. Such high-accuracy observations are extremely hard to obtain because of the need of photometric weather and the importance of obtaining several observations on different nights. In the second instalment of this paper we will use the same technique with an additional data set and combine the results. Our goal is to analyse with similar accuracy the entire 2.5-kpc volume-limited sample of Frew (2008), comprising approximately 250 central stars.

Finally, we compare the binary fraction determined here with two alternative predictions. The first one was done on the basis of PN morphology alone. De Marco & Soker (2011), revising the scheme of Soker (1997), predicted that about 60 per cent of all central stars have interacted with a stellar companion. Here we measured that 48 per cent of central stars have a companion closer than 1300 au (30 per cent $\times$ 1.45–1.69, where we took the middle of the range; Section 7.1). These two numbers are easily the same within the uncertainty, but only if all of the companions we detected (and those we did not detect but accounted for) are closer than $\sim$100 au, i.e. have interacted with the central star. The comparison is possibly closer using the *J*-band sample, whereby 67 per cent of all central stars are binaries with any separation to a distance of $\sim$1000 au.

Another prediction was that of Moe & De Marco (2011), who used a population synthesis analysis to predict that a fraction of 70 per cent of all central star derives from a binary interaction. This fraction is even higher and more discrepant with the fraction detected here for the *I*-band sample, but more in line with that derived from the *J*-band sample. All these comparisons will need to be carried out again, once the PN binary fraction is finalized and a period distribution is obtained.

ACKNOWLEDGMENTS

OD and J-CP acknowledge funding from NSF grant AST-0607111 which was used during the initial phases of this work. J-CP is thankful for Falk Herwig's support. We thank Thomas Rauch for his help in obtaining the best synthetic stellar atmospheres. We also thank Dimitri Douchin for expediting his analysis of the variability properties of the stars in our sample. We are grateful to Howard Bond for helping in the observing proposal writing stage. The TheoSSA service (http:dc.g-vo.orgtheossa) used to retrieve theoretical spectra for this paper was constructed as part of the activities of the German Astrophysical Virtual Observatory.

REFERENCES

Abell G. O., 1966, ApJ, 144, 259
Afšar M., Bond H. E., 2005, Mem. Soc. Astron. Ital., 76, 608
Bannister N. P., Barstow M. A., Holberg J. B., Bruhweiler F. C., 2003, MNRAS, 341, 477
Benedict G. F. et al., 2009, AJ, 138, 1969
Bentley A. F., 1989, in Torres-Peimbert S., ed., Proc. IAU Symp. 131, Planetary Nebulae. Kluwer, Dordrecht, p. 312
Bergeron P., Wesemael F., Beauchamp A., 1995, PASP, 107, 1047
Bessel M. S., 1990, Ap&SS, 83, 357
Bessell M. S., 1979, PASP, 91, 589
Bessell M. S., 1991, AJ, 101, 662
Bessell M. S., Brett J. M., 1988, PASP, 100, 1134
Bilíková J., Chu Y.-H., Gruendl R. A., Su K. Y. L., De Marco O., 2012, ApJS, 200, 3
Blöcker T., 1995, A&A, 299, 755
Bond H. E., 1994, in Shafter A. W., ed., ASP Conf. Ser. Vol. 56, Interacting Binary Stars. Astron. Soc. Pac., San Francisco, p. 179
Bond H. E., 2000, in Kastner J. H., Soker N., Rappaport S., eds, ASP Conf. Ser. Vol. 199, Asymmetrical Planetary Nebulae II: From Origins to Microstructures Binarity of Central Stars of Planetary Nebulae. Astron. Soc. Pac., San Francisco, p. 115

Bond H. E., Meakes M. G., Liebert J. W., Renzini A., 1993, in Weinberger R., Acker A., eds, Proc. IAU Symp. 155, Planetary Nebulae. Kluwer, Dordrecht, p. 499
Cardelli J. A., Clayton G. C., Mathis J. S., 1989, ApJ, 345, 245
Ciardullo R., Bond H. E., Sipior M. S., Fullton L. K., Zhang C.-Y., Schaefer K. G., 1999, AJ, 118, 488
Cudworth K. M., 1973, PASP, 85, 401
De Marco O., 2009, PASP, 121, 316
De Marco O., Soker N., 2011, PASP, 123, 402
De Marco O., Hillwig T. C., Smith A. J., 2008, AJ, 136, 323
De Marco O., Farihi J., Nordhaus J., 2009, J. Phys. Conf. Ser., 172, 012031
De Marco O., Passy J.-C., Moe M., Herwig F., Mac Low M.-M., Paxton B., 2011, MNRAS, 411, 2277
Dengel J., Hartl H., Weinberger R., 1980, A&A, 85, 356
Dorman B., Rood R. T., O'Connell R. W., 1993, ApJ, 419, 596
Dreizler S., 1999, Rev. Mod. Astron., 12, 255
Duquennoy A., Mayor M., 1991, A&A, 248, 485
Edgar R. G., Nordhaus J., Blackman E. G., Frank A., 2008, ApJ, 675, L101
Frew D. J., 2008, PhD thesis, Department of Physics, Macquarie University
Frew D. J., Parker Q. A., 2007, in Corradi R. L. M., Mauchado A., Soer N., eds, Asymmetrical Planetary Nebulae IV. IAC Elec. Pub., Tenerife, p. 475
Frew D. J., Parker Q. A., 2010, PASA, 27, 129
Frew D. J., Madsen G. J., O'Toole S. J., Parker Q. A., 2010, PASA, 27, 203
Frew D. J., Parker Q. A., Boijčić I., 2012, MNRAS, in press
Fulbright M. S., Liebert J., 1993, ApJ, 410, 275
García-Segura G., Langer N., Różyczka M., Franco J., 1999, ApJ, 517, 767
García-Segura G., López J. A., Franco J., 2005, ApJ, 618, 919
Gesicki K., Zijlstra A. A., 2007, A&A, 467, L29
Gianninas A., Bergeron P., Dupuis J., Ruiz M. T., 2010, ApJ, 720, 581
Good S. A., Barstow M. A., Holberg J. B., Sing D. K., Burleigh M. R., Dobbie P. D., 2004, 355, 1031
Harris H. C. et al., 2007, AJ, 133, 631
Hartl H., Dengel J., Weinberger R., 1983, Mitt. Astron. Ges., 60, 325
Henry T. J., McCarthy D. W. Jr, 1993, AJ, 106, 773
Holberg J. B., 2009, J. Phys. Conf. Ser., 172, 012022
Holberg J. B., Bergeron P., 2006, AJ, 132, 1221
Holberg J. B., Magargal K., 2005, in Koester D., Moehler S., eds, ASP Conf. Ser. Vol. 334, Finding the Cool Companions of the PG DA White Dwarfs. Astron. Soc. Pac., San Francisco, p. 419
Jacoby G. H., Ferland G. J., Korista K. T., 2001, ApJ, 560, 272
Kaler J. B., Shaw R. A., Kwitter K. B., 1990, ApJ, 359, 392
Kirkpatrick J. D., McCarthy D. W. Jr, 1994, AJ, 107, 333
Koester D., Schönberner D., 1986, A&A, 154, 125
Kraus A. L., Hillenbrand L. A., 2007, AJ, 134, 2340
Kun M., 1998, ApJS, 115, 59
Landolt A. U., 1992, AJ, 104, 340
Landolt A. U., 2009, AJ, 137, 4186
Lawrence A. et al., 2007, MNRAS, 379, 1599
Leggett S. K., 1992, ApJS, 82, 351
Liebert J., Green R., Bond H. E., Holberg J. B., Wesemael F., Fleming T. A., Kidder K., 1989, ApJ, 346, 251
Liebert J., Bergeron P., Holberg J. B., 2005, ApJS, 156, 47
Liu X.-W., Barlow M. J., Blades J. C., Osmer S., Clegg R. E. S., 1995, MNRAS, 276, 167
López J. A., Richer M. G., García-Díaz M. T., Clark D. M., Meaburn J., Riesgo H., Steffen W., Lloyd M., 2012, Rev. Mex. Astron. Astrofis., 48, 3
Lupton R., Ivezić Ž., 2005, in Seidelmann P. K., Monet A. K. B., eds, ASP Conf. Ser. Vol. 338, Astrometry in the Age of the Next Generation of Large Telescopes. Astron. Soc. Pac., San Francisco, p. 151
Madappatt N., De Marco O., Nordhaus J., Wardle M., 2011, in Schuh S., Drechsel H., Heber U., eds, AIP Conf. Ser. Vol. 1331, Towards a New Prescription for the Tidal Capture of Planets, Brown Dwarfs and Stellar Companions. Am. Inst. Phys., New York, p. 319
Maíz-Apellániz J., 2004, PASP, 116, 859
Mastrodemos N., Morris M., 1999, ApJ, 523, 357
Miszalski B., Acker A., Moffat A. F. J., Parker Q. A., Udalski A., 2009, A&A, 496, 813
Miszalski B., Acker A., Parker Q. A., Boffin H. M. J., Frew D. J., Mikolajewska J., Moffat A. F. J., Napiwotzki R., 2011, in Zijlstra A. A., Lykou F., McDonald I., Lagadec E., eds, Asymmetric Planetary Nebulae 5 Conference. Jodrell Bank Centre for Astrophysics
Moe M., De Marco O., 2006, ApJ, 650, 916
Moe M., De Marco O., 2011, in Zijlstra A. A., Lykou F., McDonald I., Lagadec E., eds, Asymmetric Planetary Nebulae 5 Conference. Jodrell Bank Centre for Astrophysics
Morales-Rueda L., Maxted P. F. L., Marsh T. R., North R. C., Heber U., 2003, MNRAS, 338, 752
Napiwotzki R., 1999, A&A, 350, 101
Napiwotzki R., Schönberner D., 1995, A&A, 301, 545
Nordhaus J., Blackman E. G., Frank A., 2007, MNRAS, 376, 599
Nordhaus J., Spiegel D. S., Ibgui L., Goodman J., Burrows A., 2010, MNRAS, 408, 631
Parker Q. A. et al., 2006, MNRAS, 373, 79
Passy J.-C. et al., 2012, ApJ, 744, 52
Raghavan D. et al., 2010, ApJS, 190, 1
Rauch T., Deetjen J. L., 2003, in Hubeny I., Mihalas D., Werner K., eds, ASP Conf. Ser. Vol. 288, Stellar Atmosphere Modeling. Astron. Soc. Pac., San Francisco, p. 103
Rauch T., Werner K., 1995, in Koester D., Werner K., eds, Lecture Notes in Physics, Vol. 443, New Analyses of Helium-Rich Pre-White Dwarfs. Springer-Verlag, Berlin, p. 186
Rauch T., Köppen J., Napiwotzki R., Werner K., 1999, A&A, 347, 169
Rauch T., Ziegler M., Werner K., Kruk J. W., Oliveira C. M., Vande Putte D., Mignani R. P., Kerber F., 2007, A&A, 470, 317
Rodríguez M., Corradi R. L. M., Mampaso A., 2001, A&A, 377, 1042
Rosado M., Moreno M. A., 1991, Ap&SS, 88, 245
Schlafly E. F., Finkbeiner D. P., 2011, ApJ, 737, 103
Schmidt-Kaler T., 1982, Bull. Inf. Cent. Donnees Stellaires, 23, 2
Schönberner D., 1983, ApJ, 272, 708
Schönberner D., 1993, in Weinberger R., Acker A., eds, Proc. IAU Symp. 155, Planetary Nebulae. Kluwer, Dordrecht, p. 415
Soker N., 1997, ApJS, 112, 487
Soker N., 2006, PASP, 118, 260
Tody D., 1986, Proc. SPIE, 627, 733
Tody D., 1993, in Hanisch R. J., Brissenden R. J. V., Barnes J., eds, ASP Conf. Ser. Vol. 52, Astronomical Data Analysis Software and Systems II. Astron. Soc. Pac., San Francisco, p. 173
Tremblay P.-E., Bergeron P., Gianninas A., 2011, ApJ, 730, 128
Tweedy R. W., Kwitter K. B., 1996, ApJS, 107, 255
Vacca W. D., Garmany C. D., Shull J. M., 1996, ApJ, 460, 914
Vassiliadis E., Wood P. R., 1994, ApJS, 92, 125
Villaver E., Livio M., 2009, ApJ, 705, L81
Wegner W., 1994, MNRAS, 270, 229
Weinberger R., Dengel J., Hartl H., Sabbadin F., 1983, ApJ, 265, 249
Werner K., 1995, Balt. Astron., 4, 340
Werner K., Dreizler S., 1999, J. Comput. Appl. Math., 109, 65
Werner K., Herwig F., 2006, PASP, 118, 183
Werner K., Deetjen J. L., Dreizler S., Nagel T., Rauch T., Schuh S. L., 2003, in Hubeny I., Mihalas D., Werner K., eds, ASP Conf. Ser. Vol. 288, Stellar Atmosphere Modeling. Astron. Soc. Pac., San Francisco, p. 31
Zuckerman B., Becklin E. E., McLean I. S., 1991, in Elston R., ed., ASP Conf. Ser. Vol. 14, Central Stars of Planetary Nebulae in the Infrared. Astron. Soc. Pac., San Francisco, p. 161

APPENDIX A: INDIVIDUAL PHOTOMETRIC MAGNITUDES OF THE CENTRAL STAR OF THE PN SAMPLE

In Table A1 we report all the photometric measurements for our central stars of PN. The measurements for each star were averaged

Table A1. The individual photometric magnitudes for our sample of PN central stars (including three PN mimics). The date and time corresponding to each night can be found in Table 3. DeHt 5 and HDW 4, having only one epoch of data, are reported only in Table 6.

Name	Night	B	V	R	I	σ_B	σ_V	σ_R	σ_I	Airmass
A7	1	15.195	15.496	15.620	–	0.014	0.012	0.011	–	1.6
	5	15.189	15.500	15.652	15.830	0.013	0.010	0.020	0.025	1.6
	7	15.188	15.491	15.635	15.808	0.012	0.009	0.019	0.021	1.5
A16	4	18.513	18.718	18.725	18.671	0.013	0.017	0.020	0.023	1.2
	5	18.535	18.729	18.758	18.707	0.015	0.013	0.021	0.028	1.4
	6	18.497	18.684	18.710	18.679	0.022	0.023	0.027	0.049	1.1
A20	4	16.214	16.468	16.551	16.681	0.011	0.014	0.018	0.018	1.2
	5	16.218	16.472	16.568	16.716	0.015	0.010	0.020	0.025	1.5
	7	16.216	16.459	16.559	16.710	0.012	0.010	0.019	0.020	1.5
A28	5	16.281	16.565	16.700	16.880	0.013	0.010	0.019	0.024	1.3
	6	16.290	16.555	16.682	16.891	0.017	0.012	0.018	0.037	1.2
	7	16.268	16.541	16.693	16.854	0.020	0.022	0.025	0.046	1.1
A31	5	15.195	15.545	15.702	15.849	0.014	0.010	0.020	0.024	1.2
	7	15.207	15.543	15.684	15.816	0.012	0.009	0.018	0.021	1.4
A57	4	17.904	17.747	17.460	17.212	0.014	0.018	0.019	0.021	1.3
	7	17.902	17.724	17.440	17.208	0.014	0.015	0.022	0.023	1.6
A71	5	19.380	19.339	19.261	19.107	0.014	0.015	0.025	0.035	1.1
	6	19.410	19.324	19.237	19.274	0.022	0.025	0.032	0.067	1.3
	7	19.372	19.338	19.258	19.201	0.013	0.013	0.024	0.038	1.1
A72	3	15.769	16.095	16.398	16.472	0.021	0.022	0.032	0.053	1.2
	4	15.740	16.028	16.165	16.358	0.013	0.016	0.020	0.024	1.6
	7	15.776	16.085	16.211	16.364	0.013	0.010	0.019	0.023	1.5
A79	3	17.813	16.961	16.404	15.814	0.015	0.014	0.018	0.026	1.2
	4	17.838	16.972	16.417	15.607	0.021	0.023	0.033	0.053	1.1
	6	17.829	16.964	16.340	15.733	0.022	0.026	0.060	0.055	1.4
A84	3	18.386	18.604	18.640	18.669	0.023	0.024	0.033	0.055	1.1
	4	18.357	18.590	18.621	18.650	0.012	0.016	0.020	0.024	1.1
	7	18.364	18.571	18.590	18.693	0.011	0.011	0.019	0.023	1.1
EGB 1	4	16.313	16.445	16.446	16.463	0.012	0.014	0.019	0.019	1.4
	5	16.301	16.434	16.460	16.507	0.015	0.011	0.022	0.024	1.4
EGB 6	4	15.691	16.001	16.129	16.292	0.011	0.014	0.018	0.018	1.2
	7	15.694	15.997	16.145	16.311	0.012	0.009	0.018	0.023	1.5
HaWe 5	4	17.310	17.444	17.469	17.536	0.012	0.011	0.010	0.015	1.0
	5	17.333	17.434	17.477	17.513	0.012	0.012	0.025	0.026	1.2
HDW 3	1	17.081	17.188	17.194	17.218	0.012	0.010	0.009	0.010	1.0
	4	17.086	17.192	17.287	17.249	0.011	0.013	0.018	0.023	1.0
	7	17.085	17.183	17.200	17.238	0.010	0.009	0.016	0.022	1.1
IsWe 1	5	16.392	16.531	16.586	16.659	0.013	0.011	0.018	0.024	1.2
	6	16.367	16.517	16.556	16.630	0.012	0.011	0.016	0.018	1.1
	7	16.360	16.517	16.592	16.650	0.020	0.022	0.025	0.046	1.1
IsWe 2	3	18.129	18.173	18.114	18.052	0.021	0.023	0.034	0.055	1.2
	4	18.124	18.168	18.120	18.101	0.024	0.015	0.020	0.025	1.2
	5	18.177	18.200	18.160	18.092	0.013	0.012	0.020	0.028	1.2
	6	18.157	18.156	18.101	18.139	0.022	0.023	0.029	0.050	1.4
	7	18.115	18.113	18.088	18.102	0.013	0.011	0.020	0.025	1.3
JnEr 1	4	16.770	17.143	17.288	17.483	0.018	0.014	0.018	0.020	1.1
	7	16.778	17.117	17.287	17.531	0.014	0.010	0.018	0.033	1.2
K 1-13	3	18.062	18.425	18.569	18.798	0.013	0.017	0.021	0.027	1.3
	4	18.045	18.420	18.603	18.896	0.013	0.013	0.020	0.030	1.2
	5	18.036	18.435	18.613	18.852	0.033	0.026	0.037	0.061	1.2
K 2-2	4	13.984	14.278	14.396	14.536	0.011	0.013	0.017	0.020	1.1
	5	13.974	14.261	14.395	14.561	0.012	0.010	0.020	0.025	1.4
	7	13.972	14.254	14.379	14.564	0.011	0.010	0.018	0.019	1.3
NGC 3587	4	15.414	15.771	15.953	16.164	0.013	0.014	0.019	0.020	1.3
	5	15.415	15.788	15.963	16.227	0.014	0.012	0.018	0.027	1.3
	6	15.413	15.768	15.966	16.207	0.021	0.023	0.027	0.047	1.3
NGC 6720	4	15.393	15.793	15.898	16.050	0.012	0.020	0.020	0.019	1.2
	7	15.420	15.747	15.904	16.075	0.016	0.019	0.022	0.022	1.6
NGC 6853	4	13.725	14.075	14.244	14.404	0.012	0.016	0.019	0.020	1.3
	5	13.777	14.100	14.241	14.390	0.012	0.013	0.019	0.045	1.1

Table A1 – *continued*

Name	Night	B	V	R	I	σ_B	σ_V	σ_R	σ_I	Airmass
	7	13.744	14.090	14.255	14.417	0.013	0.013	0.020	0.035	1.6
PuWe 1	5	15.298	15.551	15.673	15.802	0.013	0.010	0.019	0.023	1.4
	7	15.285	15.539	15.651	15.785	0.011	0.010	0.018	0.018	1.3
Sh 2-78	4	17.643	17.666	17.630	17.567	0.014	0.016	0.030	0.038	1.4
	5	17.624	17.655	17.580	17.513	0.013	0.012	0.038	0.046	1.3
Sh 2-176	3	18.639	18.580	18.597	18.602	0.022	0.024	0.036	0.059	1.1
	4	18.460	18.569	18.571	18.521	0.018	0.017	0.020	0.029	1.1
	7	18.431	18.536	18.553	18.541	0.011	0.015	0.020	0.028	1.1
Sh 2-188	4	17.438	17.454	17.407	17.361	0.012	0.014	0.017	0.019	1.1
	5	17.416	17.446	17.402	17.381	0.012	0.009	0.018	0.025	1.2
	7	17.419	17.444	17.385	17.386	0.013	0.009	0.017	0.017	1.1
Ton 320	5	15.385	15.731	15.900	16.126	0.013	0.011	0.020	0.025	1.3
	7	15.373	15.718	15.880	16.091	0.015	0.012	0.019	0.037	1.2
WeDe 1	5	16.961	17.229	17.329	17.503	0.018	0.011	0.023	0.028	1.7
	6	16.962	17.221	17.334	17.470	0.012	0.011	0.018	0.027	1.3
	7	16.946	17.231	17.354	17.500	0.021	0.022	0.027	0.046	1.1

according to equations (3) and (4) in Section 4 and presented in Table 6.

APPENDIX B: THE THEORETICAL JOHNSON–COUSINS COLOURS OF HOT STARS

In this appendix we report the colours determined for a grid of stellar atmosphere models with Solar and PG1159 abundances. The theoretical stellar atmosphere models were calculated with the simulation code TMAW, the web interface to TMAP (Werner & Dreizler 1999; Rauch & Deetjen 2003; Werner et al. 2003), or the German Astrophysical Virtual Observatory grid calculations TheoSSA[3] which are carried out for standard, non-tailored abundances but typically with a more complete model atom. TheoSSA is deemed more correct but differences were typically lower than 1 per cent. The TMAW stellar atmosphere models are calculated for a solar composition (with mass fractions $\beta_{\rm H} = 0.71$, $\beta_{\rm He} = 0.28$, $\beta_{\rm C} = 0.001$, $\beta_{\rm N} = 0.002$, $\beta_{\rm O} = 0.006$). The TheoSSA models are for $\beta_{\rm H} = 0.7$, $\beta_{\rm He} = 0.3$ unless indicated *or* for the composition typical of hydrogen-deficient PG1159 stars (Werner & Herwig 2006, $\beta_{\rm He} = 0.33$, $\beta_{\rm C} = 0.50$, $\beta_{\rm N} = 0.02$, $\beta_{\rm O} = 0.15$). The colours are then determined using the routine *calcphot* within the IRAF package (using the *vegamag* and *effstim* options). The filter system used to obtain the synthetic colours is the Johnson–Cousins system, the same as used for the determination of the standard magnitudes by Landolt (1992). These colours were modified by the zero-points listed in table 3.1 of the SYNPHOT manual, 0.010 for the $B - V$ and $R - I$ colours and -0.002 for the $V - I$ one (Maíz-Apellániz 2004; Holberg & Bergeron 2006). The $V - J$ and $J - H$ colours have not been corrected. We note that the offset for the V band alone is 0.026 mag. If the correction for the J magnitude were zero, this would imply that the theoretical colours are redder, and the resulting excess is smaller by about 3 per cent. We note that none of our detections in the $V - J$ band would be affected, although the detected spectral types would be slightly fainter. The theoretical colours for Solar as well as PG1159 abundances are tabulated in Table B1 as a function of temperature and gravity, where we have also tabulated blackbody values for comparison. The parameter space covered is that which applies to central star of PN as well as post-RGB, horizontal branch stars. See, for instance, the $\log g - T_{\rm eff}$ diagram in Napiwotzki (1999).

[3] dc.zah.uni-heidelberg.de/theossa/

APPENDIX C: THE MAGNITUDES, COLOURS AND MASSES OF MAIN-SEQUENCE STARS

In this appendix we report the value for absolute V magnitudes and colours for main-sequence stars of spectral type B3V to L0V. These data were used to interpret the I- and J-band excesses we detected in terms of companion spectral type.

For the colours of the companions (assumed to be main-sequence stars) we have used a variety of data from the literature. For spectral types earlier than B8V, we averaged the V-band absolute magnitudes and $B - V$ colours from Schmidt-Kaler (1982) and Wegner (1994), with the data from Eric Mamajek's website[4] (last updated in 2011 December). For spectral types in the range B8V–K7V, we averaged the data from Mamajek's website, Schmidt-Kaler (1982) and Kraus & Hillenbrand (2007), and transformed following Lupton & Ivezić (2005),[5] with additional $B - V$ data from Bessel (1990) and Bessell (1991). We averaged the M_V and $B - V$ data from Leggett (1992), Kirkpatrick & McCarthy (1994), Mamajek's website and Frew (unpublished) for spectral types later than M0V.

The $V - R_{\rm c}$ and colours were taken from Bessell (1979) or Bessel (1990) for spectral types earlier than M0V, and from Leggett (1992), Kirkpatrick & McCarthy (1994) and Frew (unpublished) for spectral types later than M0V. The $V - I_{\rm c}$ colours were similarly averaged from Bessell (1979), Bessel (1990), Bessell & Brett (1988), Leggett (1992), Kirkpatrick & McCarthy (1994), Mamajek's website and Frew (unpublished). The $V - J$ and $V - H$ colours were derived from Kraus & Hillenbrand (2007) and Mamajek's website for spectral types earlier than M0V, and from Kirkpatrick & McCarthy (1994), Mamajek's website and this work for spectral types later than or equal to M0V. Finally, the stellar masses were derived from the relations given in Henry & McCarthy (1993) for spectral types later than A5V, together with other literature estimates for earlier spectral types.

[4] http://www.pas.rochester.edu/~emamajek/EEM_dwarf_UBVIJHK_colors_Teff.dat

[5] http://www.sdss.org/dr5/algorithms/sdssUBVRITransform.html

Table B1. Predicted colours of single post-AGB stars using TMAP models (TMAW with solar metallicity – see the text, or TheoSSA, where the model atom and abundances are indicated as mass fractions adjacent to the relevant atom) as well as for blackbody curves (BB). These values have been adjusted for the small corrections of 0.010 mag for the $B-V$ and $R-I$ colours and −0.002 mag for the $V-I$ colours.

$T_{\rm eff}$ (kK)	log g	$B-V$ (mag)	$V-I$ (mag)	$V-J$ (mag)	$R-I$ (mag)	$J-H$ (mag)	Abundance
20	4	−0.195	−0.193	−0.466	−0.097	−0.073	Solar (TMAW)
20	5	−0.180	−0.199	−0.475	−0.099	−0.076	Solar (TMAW)
20	–	−0.139	−0.118	−0.414	−0.066	−0.068	BB
30	4	−0.269	−0.277	−0.653	−0.145	−0.109	Solar (TMAW)
30	5	−0.260	−0.280	−0.660	−0.145	−0.111	Solar (TMAW)
30	7	−0.221	−0.289	−0.680	−0.143	−0.106	Solar (TMAW)
30	8	−0.191	−0.289	−0.695	−0.139	−0.100	Solar (TMAW)
30	–	−0.226	−0.214	−0.582	−0.116	−0.098	BB
40	4	−0.271	−0.281	−0.684	−0.150	−0.114	H0.728He0.249
40	5	−0.279	−0.298	−0.713	−0.158	−0.119	H0.894He0.106
40	6	−0.274	−0.304	−0.724	−0.161	−0.121	H0.738He0.014
40	7	−0.277	−0.319	−0.759	−0.165	−0.126	Solar (TMAW)
40	8	−0.263	−0.318	−0.759	−0.161	−0.121	Solar (TMAW)
40	–	−0.266	−0.259	−0.662	−0.140	−0.113	BB
50	4	−0.280	−0.291	−0.704	−0.156	−0.116	H0.738He0.249
50	5	−0.290	−0.305	−0.725	−0.162	−0.119	H1.0
50	6	−0.298	−0.310	−0.745	−0.164	−0.125	Solar (TMAW)
50	7	−0.294	−0.316	−0.758	−0.166	−0.127	Solar (TMAW)
50	8	−0.280	−0.315	−0.760	−0.166	−0.126	H0.7He0.3
50	–	−0.289	−0.285	−0.708	−0.154	−0.122	BB
60	5	−0.302	−0.315	0.753	−0.169	−0.126	H0.7He0.3
60	6	−0.307	−0.319	−0.755	−0.169	−0.129	Solar (TMAW)
60	7	−0.305	−0.322	−0.770	−0.170	−0.130	Solar (TMAW)
60	8	−0.295	−0.322	−0.771	−0.170	−0.129	H0.7He0.3
60	–	−0.304	−0.302	−0.737	−0.163	−0.128	BB
70	5	−0.310	−0.325	−0.771	−0.174	−0.130	H0.7He0.3
70	6	−0.312	−0.323	−0.722	−0.171	−0.131	Solar (TMAW)
70	7	−0.311	−0.328	−0.780	−0.173	−0.132	Solar (TMAW)
70	8	−0.306	−0.326	−0.783	−0.175	−0.132	H0.6He0.4
70	–	−0.314	−0.314	−0.760	−0.169	−0.132	BB
80	5	−0.316	−0.331	−0.781	−0.177	−0.130	H0.7He0.3
80	6	−0.318	−0.332	−0.787	−0.178	−0.133	H0.7He0.3
80	7	−0.318	−0.333	−0.791	−0.176	−0.135	Solar (TMAW)
80	8	−0.314	−0.334	−0.797	−0.179	−0.135	H0.7He0.3
80	–	−0.322	−0.323	−0.774	−0.174	−0.135	BB
90	5	−0.316	−0.330	−0.779	−0.177	−0.129	H0.7He0.3
90	6	−0.326	−0.340	−0.806	−0.181	−0.140	Solar (TMAW)
90	7	−0.325	−0.340	−0.804	−0.180	−0.138	Solar (TMAW)
90	8	−0.322	−0.341	−0.808	−0.183	−0.137	H0.7He0.3
90	–	−0.328	−0.329	−0.786	−0.177	−0.137	BB
100	6	−0.332	−0.347	−0.817	−0.184	−0.141	Solar (TMAW)
100	7	−0.331	−0.346	−0.814	−0.183	−0.139	Solar (TMAW)
100	8	−0.329	−0.345	−0.814	−0.185	−0.138	H0.7He0.3
100	–	−0.332	−0.335	−0.796	−0.180	−0.139	BB
110	6	−0.330	−0.341	−0.801	−0.182	−0.132	H0.7He0.3
110	7	−0.336	−0.349	−0.819	−0.185	−0.140	Solar (TMAW)
110	8	−0.334	−0.347	−0.815	−0.186	−0.138	H0.7He0.3
110	–	−0.336	−0.339	−0.803	−0.182	−0.140	BB
120	6	−0.332	−0.343	−0.803	−0.183	−0.132	H0.7He0.3
120	7	−0.339	−0.352	−0.822	−0.186	−0.141	Solar (TMAW)
120	7.5	−0.337	−0.347	−0.812	−0.186	−0.136	H0.7He0.3
120	–	−0.339	−0.343	−0.810	−0.184	−0.142	BB
130	6	−0.333	−0.344	−0.804	−0.183	−0.132	H0.7He0.3
130	7	−0.341	−0.353	−0.827	−0.187	−0.142	Solar (TMAW)
130	8	−0.340	−0.350	−0.818	−0.187	−0.137	H0.7He0.3
130	–	−0.342	−0.346	−0.815	−0.186	−0.143	BB
140	6	−0.335	−0.345	−0.805	−0.184	−0.132	H0.7He0.3
140	7	−0.342	−0.354	−0.830	−0.188	−0.143	Solar (TMAW)

Table B1 – *continued*

$T_{\rm eff}$ (kK)	log g	$B-V$ (mag)	$V-I$ (mag)	$V-J$ (mag)	$R-I$ (mag)	$J-H$ (mag)	Abundance
140	8	−0.343	−0.351	−0.819	−0.188	−0.137	H0.6He0.4
140	–	−0.344	−0.348	−0.820	−0.187	−0.144	BB
150	6	−0.335	−0.346	−0.808	−0.184	−0.132	H0.7He0.3
150	7	−0.344	−0.355	−0.831	−0.188	−0.143	Solar (TMAW)
150	8	−0.343	−0.352	−0.820	−0.188	−0.137	H0.8He0.2
160	6	−0.336	−0.347	−0.810	−0.185	−0.132	H0.7He0.3
160	7	−0.345	−0.356	−0.833	−0.189	−0.144	Solar (TMAW)
160	8	−0.345	−0.353	−0.820	−0.188	−0.136	H0.7He0.3
170	6	−0.335	−0.349	−0.814	−0.185	−0.134	H0.8He0.2
170	7	−0.346	−0.358	−0.837	−0.190	−0.145	Solar (TMAW)
170	8	−0.346	−0.353	−0.821	−0.189	−0.136	H0.7He0.3
170	–	−0.349	−0.354	−0.830	−0.190	−0.146	BB
100	6	−0.307	−0.321	−0.769	−0.178	−0.151	He0.33C0.50N0.02O0.15
100	7	−0.340	−0.357	−0.835	−0.194	−0.151	He0.33C0.50N0.02O0.15
110	6	−0.369	−0.351[a]	−0.987	−0.231	−0.204	He0.33C0.50N0.02O0.15
110	7	−0.346	−0.355	−0.832	−0.194	−0.148	He0.33C0.50N0.02O0.15
120	6	−0.386	−0.382	−0.876	−0.203	−0.143	He0.33C0.50N0.02O0.15
120	7	−0.350	−0.357	−0.836	−0.195	−0.148	He0.33C0.50N0.02O0.15
130	6	−0.387	−0.384	−0.878	−0.204	−0.145	He0.33C0.50N0.02O0.15
130	7	−0.352	−0.359	−0.838	−0.196	−0.147	He0.33C0.50N0.02O0.15

[a]This colour was interpolated between the values for the 110 and 130kK atmospheres.

Table C1. Spectral types, empirical V-band absolute magnitudes, intrinsic colour indices and masses of main-sequence stars. Values followed by : are uncertain.

Spec. type	M_V (mag)	$(U-B)_0$ (mag)	$(B-V)_0$ (mag)	$(V-R_{\rm c})_0$ (mag)	$(V-I_{\rm c})_0$ (mag)	$(V-J)_0$ (mag)	$(V-H)_0$ (mag)	$(V-K_{\rm s})_0$ (mag)	Mass ($M_\odot$)
B2V	−2.10	−0.82	−0.23	−0.09	−0.23	−0.49	−0.57	−0.60	7.7
B3V	−1.45	−0.69	−0.19	−0.07	−0.19	−0.38	−0.47	−0.49	5.7
B4V	−1.22	−0.63	−0.18	−0.06	−0.18	−0.34	−0.43	−0.45	5.1
B5V	−1.06	−0.58	−0.16	−0.05	−0.17	−0.32	−0.41	−0.42	4.8
B6V	−0.77	−0.50	−0.15	−0.04	−0.15	−0.28	−0.35	−0.36	4.2
B7V	−0.53	−0.44	−0.13	−0.04	−0.11	−0.25	−0.32	−0.33	4.0
B8V	−0.24	−0.35	−0.10	−0.03	−0.09	−0.19	−0.26	−0.26	3.5
B9V	+0.16	−0.20	−0.07	−0.02	−0.06	−0.09	−0.14	−0.12	3.1
A0V	+0.79	−0.02	−0.01	+0.00	−0.01	+0.05	+0.01	+0.04	2.4
A1V	+1.05	+0.03	+0.03	+0.01	+0.03	+0.09	+0.07	+0.10	2.2
A2V	+1.36	+0.06	+0.06	+0.03	+0.07	+0.17	+0.16	+0.19	2.1
A3V	+1.53	+0.08	+0.09	+0.05	+0.10	+0.20	+0.20	+0.23	2.0
A4V	+1.74	+0.09	+0.13	+0.06	+0.17	+0.30	+0.32	+0.36	1.95
A5V	+1.90	+0.10	+0.15	+0.07	+0.19	+0.36	+0.37	+0.40	1.89
A7V	+2.16	+0.10	+0.20	+0.12	+0.24	+0.45	+0.49	+0.53	1.76
A8V	+2.35	+0.09	+0.25	+0.15	+0.29	+0.51	+0.59	+0.63	1.65
F0V	+2.63	+0.04	+0.30	+0.18	+0.36	+0.60	+0.69	+0.73	1.58
F2V	+3.00	−0.00	+0.36	+0.21	+0.43	+0.72	+0.88	+0.93	1.46
F5V	+3.46	−0.02	+0.43	+0.27	+0.52	+0.89	+1.03	+1.08	1.31
F8V	+4.01	+0.01	+0.53	+0.30	+0.60	+1.06	+1.23	+1.29	1.19
G0V	+4.40	+0.05	+0.58	+0.33	+0.67	+1.12	+1.36	+1.42	1.10
G2V	+4.72	+0.12	+0.64	+0.36	+0.71	+1.18	+1.47	+1.55	1.03
G5V	+5.07	+0.19	+0.67	+0.39	+0.74	+1.25	+1.56	+1.64	0.99
G8V	+5.51	+0.29	+0.74	+0.43	+0.78	+1.38	+1.69	+1.77	0.93
K0V	+5.89	+0.44	+0.82	+0.46	+0.85	+1.50	+1.86	+2.03	0.87
K1V	+6.08	+0.52	+0.85	+0.50	+0.88	+1.55	+1.94	+1.95	0.85
K2V	+6.37	+0.62	+0.90	+0.54	+0.93	+1.67	+2.06	+2.16	0.82
K3V	+6.61	+0.80	+0.98	+0.57	+1.05	+1.81	+2.30	+2.41	0.80
K5V	+7.34	+1.08	+1.16	+0.73	+1.29	+2.19	+2.71	+2.84	0.72
K7V	+8.16	+1.20	+1.34	+0.81	+1.57	+2.54	+3.24	+3.41	0.65
M0V	+8.87	+1.19	+1.41	+0.89	+1.76	+2.86	+3.50	+3.74	0.59

Table C1 – *continued*

Spec. type	M_V (mag)	$(U-B)_0$ (mag)	$(B-V)_0$ (mag)	$(V-R_c)_0$ (mag)	$(V-I_c)_0$ (mag)	$(V-J)_0$ (mag)	$(V-H)_0$ (mag)	$(V-K_s)_0$ (mag)	Mass ($M_\odot$)
M1V	+9.56	+1.18	+1.47	+0.96	+1.98	+3.20	+3.77	+4.03	0.54
M2V	+10.17	+1.17	+1.50	+1.00	+2.14	+3.36	+3.94	+4.18	0.45
M3V	+11.01	+1.17	+1.55	+1.08	+2.45	+3.80	+4.38	+4.62	0.33
M4V	+12.80	+1.18	+1.67	+1.19	+2.75	+4.41	+4.96	+5.23	0.24
M5V	+14.20	+1.3:	+1.82	+1.41	+3.30	+5.13	+5.73	+6.00	0.15
M6V	+16.59	+1.3:	+2.03	+1.81	+3.93	+6.25	+6.86	+7.19	0.11
M7V	+17.84	–	+2.15	+2.13	+4.51	+7.03	+7.64	+8.02	0.10
M8V	+18.72	–	+2.15	+2.24	+4.57	+7.55	+8.23	+8.67	0.09
M9V	+19.39	–	+2.15	+2.37	+4.61	+7.72	+8.45	+8.94	0.08
L0V	+19.65	–	–	+2.44	+4.66	+8.10	+8.82	+9.36	0.08

This paper has been typeset from a TEX/LATEX file prepared by the author.

Royal Astronomical Society. Monthly Notices

Title Details | Table of Contents

Basic Description

Title	Royal Astronomical Society. Monthly Notices
ISSN	0035-8711
Publisher	Oxford University Press
Country	United Kingdom
Status	Active
Start Year	1827
Frequency	36 times a year
Language of Text	Text in: English
Refereed	Yes
Abstracted / Indexed	Yes
Serial Type	Journal
Content Type	Academic / Scholarly
Format	Print
Website	http://www.oxfordjournals.org/our_journals/mnras/
Description	Publishes the results of original research in positional and dynamical astronomy, astrophysics, radio astronomy, cosmology, space research and the design of astronomical instruments.

Subject Classifications
Additional Title Details
Title History Details
Publisher & Ordering Details
Price Data
Online Availability
Abstracting & Indexing
Other Availability
Demographics
Reviews

Save to List Email Download Print Corrections Expand All Collapse All